

Wave kinetics in an integrable model – the Kaup-Boussinesq system

Ashleigh Simonis*

*Department of Naval Architecture and Marine Engineering,
University of Michigan, 2600 Draper Drive, Ann Arbor, Michigan 48109, USA*

Sergey Nazarenko

Institut de Physique de Nice, Université Côte d'Azur et CNRS, 17 rue Julien Lauprêtre, 06200 Nice, France

Jalal Shatah

*Courant Institute of Mathematical Sciences, New York University,
251 Mercer Street, New York, New York 10012, USA*

Yulin Pan†

*Department of Naval Architecture and Marine Engineering,
University of Michigan, 2600 Draper Drive, Ann Arbor, Michigan 48109, USA*

(Dated: January 14, 2026)

We study wave turbulence in one-dimensional (1-D) bidirectional shallow water waves described by the Kaup-Boussinesq (KB) equation, which is known to be an integrable system. In contrast to the generally accepted empirical belief that an integrable system yields no kinetic theory, we derive and validate a non-trivial wave kinetic equation (WKE) for the KB system with a non-zero interaction coefficient on the four-wave resonant manifold. This WKE is non-homogeneous in nature due to the non-homogeneity in the dispersion relation of the KB system; however, approximate Kolmogorov-Zakharov (KZ) solutions can be derived in a novel way under certain approximations. We numerically verify the theoretical findings in two cases: (i) In free-evolution cases, although the discrete (nonlinear) spectrum remains unchanged as guaranteed by an integrable system's isospectrality, an initial arbitrary wavenumber spectrum quickly evolves into a thermo-equilibrium state, demonstrating the kinetic aspect of the system; (ii) in forced-dissipated cases, we find stationary power-law spectra that agree with the theoretical predictions.

I. INTRODUCTION

Integrability theory and wave kinetic theory are typically viewed as opposite ends of dispersive partial differential equations. For integrable systems, the dynamics are characterized by a set of conserved quantities, resulting in deterministic and stable solutions that do not thermalize. In contrast, wave kinetic theory describes the long-term statistical behavior of weakly nonlinear wave systems, predicting the irreversible evolution of a wave spectrum toward either a thermal equilibrium state or a Kolmogorov-Zakharov (KZ) turbulent state [e.g., 1, 2]. It is a widely held empirical belief in the field (despite a lack of rigorous proofs) that if a system is integrable, it should yield no kinetic theory, and vice versa. This concept has been presumed to apply to all integrable models, such as the one-dimensional (1-D) nonlinear Schrödinger equation (NLS), the Korteweg-de Vries (KdV) equation, and others that span many domains of physics.

The purpose of this paper is to challenge the above “standard” view of integrability and wave kinetic theory through a special case of the Kaup-Boussinesq (KB) system, which is known to be a completely integrable system (in the sense that it can be completely solved by the clas-

sical inverse scattering method [e.g., 3–8]) that describes 1-D bidirectional shallow water waves. Before discussing the water wave problem and the KB system, we note that Zakharov [9] has mentioned, contrary to the general belief, certain types of “weakly” integrable systems capable of yielding non-trivial kinetic behavior. In his notion, such systems admit a non-trivial wave kinetic equation (WKE) with an infinite number of invariants. For example, the well-known Kadomtsev-Petviashvili-1 equation is a weakly integrable system [9]. The KB system, however, does not belong to this class because its WKE does not have (or is not known to possess) an infinite number of invariants, which is one of the key properties outlined in that work.

We start by remarking that wave kinetic theory has been relatively well developed for deep water waves, starting from the derivation of the Hasselmann's WKE [10]. It is well established that wave turbulence in deep water with 1- and 2-D free surfaces is governed by five [e.g., 11–13] and four-wave [e.g., 10, 14–16] resonant interactions, respectively. In comparison, the theoretical development of shallow-water wave turbulence remains relatively underexplored in the literature. The theory for 2-D shallow-water surface waves has been developed starting from either the Euler equations [17] or the Boussinesq equations [18], with their predictions of the KZ spectrum observed in wave tank experiments [19]. In 1-D cases, however, many contend that there is no need to study

* asimonis@umich.edu

† yulinp@umich.edu

wave turbulence, as the dynamics are governed by integrable models (such as the KdV equation) and non-trivial resonances are thought to be absent [e.g., 1, 17].

It should be noted that the KdV equation formulation is for unidirectional wave propagation. Allowing bidirectional propagation in 1-D seems to render the system “less integrable”, as it allows for four-wave resonant interactions (see §II A for details). However, because the bidirectional dynamics are captured by the integrable KB system mentioned above, the general consensus is that there is still no wave turbulence. This appears to contradict experimental studies of bidirectional shallow water waves [e.g., 20–22] that show spectral evolution toward a flat energy spectrum at large scales (interpreted as thermalization in [23]) and/or the emergence of a soliton gas, depending on the system nonlinearity and forcing condition. On the other hand, there are non-integrable 1-D Boussinesq equations (some of which are far from integrable, e.g., [18] when reduced to 1-D) that predict the kinetic behavior of waves. In any case, it is problematic to regard the KB equation as a unique model for 1-D bidirectional shallow water waves, yet it explains only a subset of experimental observations, i.e., those displaying integrable features.

It is based on the above reasoning that we hypothesize that the KB model may yield a non-trivial kinetic description, similar to that emerging from other non-integrable Boussinesq-type equations. In this paper, we derive a WKE from the KB model and find that the interaction coefficients on the four-wave resonant manifold are non-zero, indicating that the system has non-trivial kinetic behavior. The derivation involves a normal form transformation to remove the quadratic terms in the KB equation, for which we carefully characterize its validity condition depending on the parameters α and β measuring the nonlinearity and dispersion. The resulting WKE is inherently non-homogeneous due to the inhomogeneity of the KB dispersion relation. While the thermal equilibrium spectra remain as exact stationary solutions, the KZ solutions must be derived under approximations in a novel way. We derive two distinct direct cascade solutions corresponding to the limits of small and large modal amplitudes at low wavenumbers, given respectively by $n_k \sim |k|^{-3}$ and $n_k \sim |k|^{-3/2}$, with each corresponding to a local solution of the WKE.

We proceed to perform direct numerical simulations of the KB equation to test the validity of our theoretical predictions. We start by demonstrating a free-evolution case from random-wave initial conditions, where the discrete eigenvalues obtained from the direct scattering transform (representing solitons present in the initial field) remain constant in time, while the wavenumber spectrum quickly evolves toward a thermalized state. This case provides compelling evidence for the coexistence of integrable and wave-kinetic features in the KB system—the former reflected by the isospectrality of the eigenvalues, and the latter by the thermalization of the wave spectrum. We then study the free-evolution problem by systematically

varying the nonlinearity α and show that the thermalization phenomenon holds across a broad range of α , including those at very weak nonlinearity. Finally, we perform numerical simulations of the forced-dissipated KB system while controlling the low-wavenumber modal amplitude through the presence of the low-wavenumber dissipation. For small and large modal amplitudes at low wavenumbers, respectively, we reproduce the two theoretical KZ solutions.

We finally remark that the wave kinetic behavior we discover in the present paper is fundamentally different from what is referred to as “integrable turbulence” [e.g., 24–30]. “Integrable turbulence” may refer to a soliton gas state in an integrable model, associated with a kinetic equation that describes the statistical properties of the ensemble of solitons, rather than the free waves considered in this work. The present study also differs from previous works in which an integrable model needs to be slightly modified to create a near-integrable system that exhibits wave turbulence, e.g., from the integrable Toda lattice problem to the α -FFPUT problem, where the latter thermalizes [31]. To the authors’ knowledge, the emergence of wave turbulence from an integrable system, as demonstrated in this work, is entirely new and is likely unexpected by many in the nonlinear science community. We will conclude this paper by highlighting several distinctive features of the KB system, such as its mathematical ill-posedness at high wavenumbers and the non-self-adjoint nature of the spectral operator in its Lax pair. We will also discuss the general relationship between integrability and kinetic theory, illustrating a connection that has been largely overlooked but has considerable potential to inspire new research directions.

II. THEORETICAL DERIVATION

A. Derivation of the wave kinetic equation

We begin with the Kaup-Boussinesq (KB) system

$$\eta_t + [(h + \eta)u]_x = -\frac{h^3}{3}u_{xxx}, \quad (1)$$

$$u_t + uu_x + g\eta_x = 0, \quad (2)$$

where $\eta(x, t)$ denotes the surface elevation, $u(x, t)$ is the fluid velocity, g is the acceleration of gravity, and h is the water depth. The system of (1) and (2) is known to be completely integrable in the inverse scattering method (ISM) sense [3]. We introduce the following non-dimensional variables:

$$\tilde{\eta} = \eta/a, \quad \tilde{x} = x/L_p, \\ \tilde{t} = t/(L_p/\sqrt{gh}), \quad \tilde{u} = u/(\sqrt{gh}\frac{a}{h}). \quad (3)$$

where a denotes the characteristic wave amplitude (e.g., half the significant wave height H_s) and L_p is the peak

wavelength of the wave field. Substituting (3) into (1) and (2) and omitting the tilde notation, we obtain

$$\eta_t + u_x + \alpha(\eta u)_x = -\frac{1}{3}\beta u_{xxx}, \quad (4)$$

$$u_t + \eta_x + \alpha u u_x = 0, \quad (5)$$

where $\alpha = a/h$ and $\beta = (h/L_p)^2$ are dimensionless measures of nonlinearity and dispersion, respectively.

We consider (4) and (5) on a periodic domain \mathbb{T}_L . Defining Fourier-domain variables such as $\hat{\eta}_k(t) = \int_0^L \eta(x, t) e^{-ikx} dx / L$ (note that k can be positive or negative), (4) and (5) can be transformed into:

$$\frac{\partial \hat{\eta}_k}{\partial t} + i(k - \frac{1}{3}\beta k^3) \hat{u}_k + i\alpha \sum_{k_1+k_2=k} k \hat{\eta}_{k_1} \hat{u}_{k_2} = 0, \quad (6)$$

$$\frac{\partial \hat{u}_k}{\partial t} + ik\hat{\eta}_k + \frac{i}{2}\alpha \sum_{k_1+k_2=k} k \hat{u}_{k_1} \hat{u}_{k_2} = 0. \quad (7)$$

The linear part of (6) and (7) yields the dispersion relation

$$\omega_k = \kappa \sqrt{1 - \frac{1}{3}\beta\kappa^2} \approx \kappa(1 - \frac{1}{6}\beta\kappa^2), \quad (8)$$

where $\kappa = |k|$, and we assume that the dispersion is small, i.e., $\beta\kappa^2 \ll 1$.

By defining the canonical variables,

$$\hat{\eta}_k = \frac{\sqrt{2}}{2} \omega_k^{1/2} (a_k + a_{-k}^*) \quad (9)$$

and

$$\hat{u}_k = \frac{\sqrt{2}}{2} \frac{k}{\omega_k^{1/2}} (a_k - a_{-k}^*), \quad (10)$$

leading to

$$a_k = \frac{\sqrt{2}}{2} \omega_k^{-1/2} \hat{\eta}_k + \frac{\sqrt{2}}{2} \frac{\omega_k^{1/2}}{k} \hat{u}_k, \quad (11)$$

we can diagonalize (6) and (7) in the variable a_k

$$\begin{aligned} \frac{\partial a_k}{\partial t} + i\omega_k a_k + \frac{i\alpha}{4\sqrt{2}} \sum_{k_1+k_2=k} \{U_{k12} a_{k_1} a_{k_2} - U_{k12} a_{k_1} a_{-k_2}^* \\ + S_{k12} a_{-k_1}^* a_{k_2} - S_{k12} a_{-k_1}^* a_{-k_2}^*\} = 0, \end{aligned} \quad (12)$$

where

$$U_{k12} = [2W(k, 2) + W(1, 2)](\omega_k \omega_{k_1} \omega_{k_2})^{1/2}, \quad (13)$$

$$S_{k12} = [2W(k, 2) - W(1, 2)](\omega_k \omega_{k_1} \omega_{k_2})^{1/2}, \quad (14)$$

with

$$\begin{aligned} W(i, j) = & \operatorname{sgn}(k_i) \operatorname{sgn}(k_j) \\ & \times (1 - \frac{\beta}{3} k_i^2)^{-1/2} (1 - \frac{\beta}{3} k_j^2)^{-1/2}. \end{aligned} \quad (15)$$

Manipulating (12) using symmetry conditions, we get the final canonical equation

$$\begin{aligned} \frac{\partial a_k}{\partial t} + i\omega_k a_k + i\{ & \sum_{k_1+k_2=k} V_{k12} a_{k_1} a_{k_2} \\ & + \sum_{k_1-k_2=k} V_{k12} a_{k_1} a_{k_2}^* + \sum_{k_2-k_1=k} V_{k12} a_{k_1}^* a_{k_2} \\ & + \sum_{k_2+k_1=k} V_{k12} a_{k_1}^* a_{k_2}^* \} = 0, \end{aligned} \quad (16)$$

where

$$V_{k12} = \frac{\alpha(\omega_k \omega_{k_1} \omega_{k_2})^{1/2}}{4\sqrt{2}} [W(k, 1) + W(k, 2) + W(1, 2)]. \quad (17)$$

We note that all interaction kernels in (16) are the same, which is consistent with the case in the 2-D Boussinesq equation derived in [18].

Our next goal is to apply a normal form transformation (or multiple time scale method) to (16) with the aim of eliminating the quadratic nonlinear terms, since the dispersion relation (8) does not support triad resonant interactions. This approach has been previously applied to the 2-D Euler equations for shallow water [17] and to the 2-D Boussinesq equations [18]. The procedure is standard [e.g., 1, 32] except for the validity condition of the transformation, which will be discussed later.

We proceed by applying the normal form transformation method to introduce a new variable b_k defined as

$$\begin{aligned} a_k = b_k + \sum_{k_1+k_2=k} \Gamma_{k12}^{[1]} b_{k_1} b_{k_2} - 2 \sum_{k_2-k_1=k} \Gamma_{2k1}^{[1]} b_{k_1}^* b_{k_2} \\ + \sum_{k_1+k_2+k=0} \Gamma_{k12}^{[2]} b_{k_1}^* b_{k_2}^* + \sum_{k+k_1=k_2+k_3} B_{0123} b_{k_1}^* b_{k_2} b_{k_3} \\ + \text{other cubic terms}, \end{aligned} \quad (18)$$

such that rewriting (16) in terms of b_k yields

$$\frac{\partial b_k}{\partial t} + i\omega_k b_k + i \sum_{k+k_1=k_2+k_3} T_{k123} b_{k_1}^* b_{k_2} b_{k_3} = 0. \quad (19)$$

This transformation is achieved by appropriately choosing the coefficients in (18), for example,

$$\Gamma_{k12}^{[1]} = \frac{-V_{k12}}{\omega_k - \omega_1 - \omega_2}, \quad \Gamma_{k12}^{[2]} = \frac{-V_{k12}}{\omega_k + \omega_1 + \omega_2}.$$

The interaction kernel in (19) is given by

$$\begin{aligned}
T_{k123} = & -V_{k,2,k-2}V_{3,1,3-1} \left[\frac{1}{\omega_2 + \omega_{k-2} - \omega_k} + \frac{1}{\omega_1 + \omega_{3-1} - \omega_3} \right] \\
& - V_{1,2,1-2}V_{3,k,3-k} \left[\frac{1}{\omega_2 + \omega_{1-2} - \omega_1} + \frac{1}{\omega_k + \omega_{3-k} - \omega_3} \right] \\
& - V_{k,3,k-3}V_{2,1,2-1} \left[\frac{1}{\omega_3 + \omega_{k-3} - \omega_k} + \frac{1}{\omega_1 + \omega_{2-1} - \omega_2} \right] \\
& - V_{1,3,1-3}V_{2,k,2-k} \left[\frac{1}{\omega_3 + \omega_{1-3} - \omega_1} + \frac{1}{\omega_k + \omega_{2-k} - \omega_2} \right] \\
& - V_{k+1,k,1}V_{2+3,2,3} \left[\frac{1}{\omega_{k+1} - \omega_k - \omega_1} + \frac{1}{\omega_{2+3} - \omega_2 - \omega_3} \right] \\
& - V_{-k-1,k,1}V_{-2-3,2,3} \left[\frac{1}{\omega_{k+1} + \omega_k + \omega_1} + \frac{1}{\omega_{2+3} + \omega_2 + \omega_3} \right].
\end{aligned} \tag{20}$$

We observe that T_{k123} in (20) possesses the desired symmetry properties, namely, $T_{k123} = T_{1k23} = T_{k132} = T_{23k1}$.

To obtain the above results, the transformation $a_k \rightarrow b_k$ defined in (18) must be near-identity. As discussed in [17], this requires

$$\begin{aligned}
& \left| \sum_{k_1+k_2=k} \Gamma_{k12}^{[1]} b_{k_1} b_{k_2} - 2 \sum_{k_2-k_1=k} \Gamma_{2k1}^{[1]} b_{k_1}^* b_{k_2} \right. \\
& \left. + \sum_{k_1+k_2+k=0} \Gamma_{k12}^{[2]} b_{k_1}^* b_{k_2}^* \right| \ll |b_k|
\end{aligned} \tag{21}$$

In formulating (21), inconsistencies arise in [17]. In particular, the analysis in [17] does not account for the random phases of b_k when estimating the summations on the left-hand side, resulting in an overestimation. In Appendix A, we provide a new estimation that properly incorporates phase randomness to derive the validity condition for the normal form transformation (see also [33]). The result is straightforward and can be summarized as follows:

We consider a spectrum with finite bandwidth Δ in k , assuming that it decays sufficiently fast outside Δ . Then (21) corresponds to the condition of $\alpha \ll \beta$. While the detailed derivation is provided in Appendix A, the underlying logic is to avoid small denominators arising on the left-hand side of (21). The most singular term in the denominator is of $O(\beta)$, which must be significantly larger than the numerator of $O(\alpha)$.

Starting from (19), we formally derive the corresponding wave kinetic equation (WKE) following standard procedures [e.g., 2]. The WKE is given by

$$\begin{aligned}
\frac{\partial n_k}{\partial t} = & 4\pi \int |T_{k123}|^2 n_k n_1 n_2 n_3 \left[\frac{1}{n_k} + \frac{1}{n_1} - \frac{1}{n_2} - \frac{1}{n_3} \right] \\
& \times \delta(k + k_1 - k_2 - k_3) \delta(\omega_k + \omega_1 - \omega_2 - \omega_3) dk_1 dk_2 dk_3,
\end{aligned} \tag{22}$$

where $n_k = \langle b_k b_k^* \rangle \approx \langle a_k a_k^* \rangle$ denotes the wave action.

To determine whether (22) is trivial or not, it is essential to analyze the interaction coefficient T_{k123} on the resonant manifold defined by the resonance condition in

(22). We first emphasize that for any concave-down dispersion relation, such as (8), the resonance condition in frequency ω cannot be satisfied if all involved wavenumbers share the same sign (i.e., all positive or all negative). Resonant interactions can only occur when exactly one wavenumber has a sign opposite to the other three (for example, one negative and three positive wavenumbers). A graphical proof of this fact is provided in Appendix B, which is fundamental to the subsequent analysis of T_{k123} .

The existing view for the shallow-water wave interaction coefficient, such as (20), is that it contains both near-singular and regular terms [17, 18]. The former correspond to frequency mismatches of $O(\beta)$ (i.e., their inverses are $O(1/\beta)$, which is near-singular), while the latter are of $O(1)$. It has previously been thought that the near-singular terms dominate the coefficient T_{k123} . However, we find this previous understanding incorrect after a careful calculation, as outlined below.

Without loss of generality, we consider k, k_1, k_2 to be positive and k_3 to be negative, such that $\kappa_2 > \kappa, \kappa_1, \kappa_3$. Under this assumption, the “near-singular” and “regular” terms in (20) (hereafter named as T_I and T_{II}) can be collected as

$$\begin{aligned}
T_I = & -\frac{V_{k,3,k-3}V_{2,1,2-1}}{\omega_1 + \omega_{2-1} - \omega_2} - \frac{V_{1,3,1-3}V_{2,k,2-k}}{\omega_k + \omega_{2-k} - \omega_2} \\
& - \frac{V_{k+1,k,1}V_{2+3,2,3}}{\omega_{k+1} - \omega_k - \omega_1},
\end{aligned} \tag{23}$$

$$T_{II} = T_{k123} - T_I.$$

Substitution of (8) and (17) into (23) gives (see details in Appendix C)

$$\begin{aligned}
T_I = & -\frac{3\alpha^2}{16\beta} \left(\frac{\kappa_3^3}{\kappa\kappa_1\kappa_2} \right)^{1/2}, \\
T_{II} = & \frac{3\alpha^2}{64} (\kappa\kappa_1\kappa_2\kappa_3)^{1/2} \left[\kappa_3 \left(\frac{1}{\kappa_1} + \frac{1}{\kappa} - \frac{1}{\kappa_2} \right) + 6 \right].
\end{aligned} \tag{24}$$

In fact, from (24) it seems that $T_I \ll T_{II}$ for small β . However, solving the resonance condition in (22) gives $\kappa_3 = (\beta/4)\kappa\kappa_1\kappa_2$ (see Appendix C), substitution of which into (24) shows that T_I and T_{II} both scale with

$\sqrt{\beta}$ at the leading order:

$$T_{\text{I}} = -\frac{3\alpha^2}{128}\sqrt{\beta}\kappa\kappa_1\kappa_2, \quad T_{\text{II}} = \frac{9\alpha^2}{64}\sqrt{\beta}\kappa\kappa_1\kappa_2. \quad (25)$$

Thus, T_{k123} takes the compact form

$$T_{k123} = \frac{15\alpha^2}{128}\sqrt{\beta}\kappa\kappa_1\kappa_2. \quad (26)$$

We note that if any wavenumber other than k_3 is chosen to be negative (with the others positive), the coefficient T_{k123} can be directly evaluated using its symmetry properties. For example, if $k_1 < 0$, one can use the relation $T_{k123} = T_{231k}$, where the latter evaluates to $T_{231k} = (15\alpha^2/128)[\sqrt{\beta}\kappa\kappa_2\kappa_3]$. Consequently, a general expression for T_{k123} can be written as

$$T_{k123} = \frac{15\alpha^2}{128}\left(\sqrt{\beta}\kappa_{\text{mul}}\right), \quad (27)$$

where κ_{mul} represents the multiplication of the magnitudes of the three wavenumbers with the same sign.

We also remark here that it is claimed in [17] that all “near-singular” terms in T_{k123} cancel out, based on the formulation from the Euler equation. This claim is in fact not relevant to the present case, since [17] assumes that all wavenumbers share the same sign, which is not consistent with the resonant manifold in (22).

Since $T_{k123} \neq 0$ on the resonant manifold according to (27), we have obtained a non-trivial WKE (22) from the integrable model (4) and (5). Next, we seek stationary solutions to (22). The first set of stationary solutions is of Rayleigh-Jean type, namely the equipartition-of-action solution $n_k \sim \kappa^0$ and the equipartition-of-energy solution $n_k \sim 1/\omega_k \cong 1/\kappa^1$. These naturally hold for (22) since they turn the integrand in the integral on the right-hand side into zero at each point. However, the Kolmogorov-Zakharov turbulent solution to (22) needs to be found in a novel way, which we describe in the following section.

B. Kolmogorov-Zakharov spectra

One might attempt to find the KZ solution $n_k \sim \kappa^\gamma$ to (22) using a “standard” approach using the formula $\gamma = -2\tau/3 - 1$ [2] with τ the degree of homogeneity of T_{k123} . However, this approach does not hold here because the dispersion relation (8) is inhomogeneous, which breaks the basis to derive the “standard” formula. As one may have noticed here, even the degree of homogeneity τ is not certain here depending on whether (24) or (25) is used for evaluation, which results from the same inhomogeneity issue. If one simply considers a dispersion relation $\omega_k = \kappa$ with $\beta = 0$, then the resonance condition leads to $\kappa_3 = 0$ in (24) so that $T_{k123} = 0$ and the problem becomes trivial. Therefore, to obtain the KZ spectrum, we have to develop a refined approach which considers the cubic terms in the dispersion relation (as we have done in deriving (25)).

We start by considering an isotropic spectrum, $n_{-\kappa} = n_\kappa$, which allows us to convert wavenumber k into its magnitude κ in (22). In particular, the resonance condition in k permits eight sign choices for k_1 , k_2 and k_3 (for fixed positive k), but disregarding trivial pairings (e.g., $k = k_2$, $k_1 = k_3$; $k_1 = k_2$, $k = k_3$) leaves only four non-trivial cases where the integrand is non-zero. The resulting equation in κ is

$$\begin{aligned} \frac{\partial n_\kappa}{\partial t} = 4\pi \int & |T_{k123}|^2 n_\kappa n_1 n_2 n_3 \left[\frac{1}{n_\kappa} + \frac{1}{n_1} - \frac{1}{n_2} - \frac{1}{n_3} \right] \\ & \times \delta(\omega_\kappa + \omega_1 - \omega_2 - \omega_3) [\delta(\kappa + \kappa_1 - \kappa_2 + \kappa_3) \\ & + \delta(\kappa + \kappa_1 + \kappa_2 - \kappa_3) + \delta(\kappa - \kappa_1 - \kappa_2 - \kappa_3) \\ & + \delta(\kappa - \kappa_1 + \kappa_2 + \kappa_3)] d\kappa_1 d\kappa_2 d\kappa_3. \end{aligned} \quad (28)$$

We name the four terms in (28) I_1 , I_2 , I_3 , and I_4 , corresponding to the four delta functions in the square brackets. To further simplify I_1 associated with $\delta(\kappa + \kappa_1 - \kappa_2 + \kappa_3)$ in (28) (as an example), we notice that the frequency resonance condition can be reduced to (see Appendix D 1)

$$\omega_\kappa + \omega_1 - \omega_2 - \omega_3 \approx \kappa_3 - \frac{\beta}{4}\kappa\kappa_1\kappa_2. \quad (29)$$

The wavenumber resonance condition is reduced to $\kappa + \kappa_1 - \kappa_2 + O(\beta)$, with the $O(\beta)$ term negligible at leading order. Therefore, integrating out the frequency condition and using (27) reduces I_1 to

$$\begin{aligned} I_1 = \int & \left| \frac{15\alpha^2}{128}\sqrt{\beta}\kappa\kappa_1\kappa_2 \right|^2 n_\kappa n_1 n_2 n_3 \\ & \times \left[\frac{1}{n_\kappa} + \frac{1}{n_1} - \frac{1}{n_2} - \frac{1}{n_3} \right] \delta(\kappa + \kappa_1 - \kappa_2) d\kappa_1 d\kappa_2. \end{aligned} \quad (30)$$

Following similar procedures, we can reduce I_2 and I_3 to

$$\begin{aligned} I_2 = \int & \left| \frac{15\alpha^2}{128}\sqrt{\beta}\kappa\kappa_1\kappa_3 \right|^2 n_\kappa n_1 n_2 n_3 \\ & \times \left[\frac{1}{n_\kappa} + \frac{1}{n_1} - \frac{1}{n_2} - \frac{1}{n_3} \right] \delta(\kappa + \kappa_1 - \kappa_3) d\kappa_1 d\kappa_3 \end{aligned} \quad (31)$$

and

$$\begin{aligned} I_3 = \int & \left| \frac{15\alpha^2}{128}\sqrt{\beta}\kappa\kappa_2\kappa_3 \right|^2 n_\kappa n_1 n_2 n_3 \\ & \times \left[\frac{1}{n_\kappa} + \frac{1}{n_1} - \frac{1}{n_2} - \frac{1}{n_3} \right] \delta(\kappa - \kappa_2 - \kappa_3) d\kappa_2 d\kappa_3, \end{aligned} \quad (32)$$

respectively. For I_4 , the frequency condition cannot be satisfied for $\kappa \sim O(1)$, thus $I_4 = 0$ and does not contribute to (28).

Integrals (30)-(32) can be further simplified depending on the size of n_κ at $\kappa \sim \beta$ relative to n_κ in the inertial

range. In what follows, we discuss two cases: Cases A and B with n_κ respectively small and large in the vicinity of $\kappa \sim \beta$. These two cases physically correspond to situations with and without large-scale damping in the simulations demonstrated in section §III B 2.

1. Case A

Consider I_1 with $n_3 \ll n_\kappa, n_1, n_2$, the integral in (30) can be reformulated as (with $1/n_3$ term dominating over other terms in the square bracket)

$$I_1 = - \int \left| \frac{15\alpha^2}{128} \sqrt{\beta} \kappa \kappa_1 \kappa_2 \right|^2 n_\kappa n_1 n_2 \delta(\kappa + \kappa_1 - \kappa_2) d\kappa_1 d\kappa_2, \quad (33)$$

Similar procedures applied to I_2 and I_3 reduce (31) and (32) to

$$I_2 = - \int \left| \frac{15\alpha^2}{128} \sqrt{\beta} \kappa \kappa_1 \kappa_3 \right|^2 n_\kappa n_1 n_3 \delta(\kappa + \kappa_1 - \kappa_3) d\kappa_1 d\kappa_3, \quad (34)$$

and

$$I_3 = \int \left| \frac{15\alpha^2}{128} \sqrt{\beta} \kappa \kappa_2 \kappa_3 \right|^2 n_\kappa n_2 n_3 \delta(\kappa - \kappa_2 - \kappa_3) d\kappa_2 d\kappa_3. \quad (35)$$

By defining

$$R_{12}^\kappa = \left| \frac{15\alpha^2}{128} \sqrt{\beta} \kappa \kappa_1 \kappa_2 \right|^2 n_\kappa n_1 n_2 \delta(\kappa - \kappa_2 - \kappa_1) \quad (36)$$

the integral I can be expressed as

$$I = I_1 + I_2 + I_3 = \int (R_{12}^\kappa - R_{1\kappa}^2 - R_{\kappa 2}^1) d\kappa_1 d\kappa_2. \quad (37)$$

After applying the Zakharov transformations [1] and assuming a solution ansatz $n_\kappa \sim \kappa^{-x}$ (see Appendix D 2 for full details), we can write (37) as

$$I = \int R_{12}^\kappa \left[1 - \left(\frac{\kappa_1}{\kappa} \right)^{3x-8} - \left(\frac{\kappa_2}{\kappa} \right)^{3x-8} \right] d\kappa_1 d\kappa_2. \quad (38)$$

The condition for a stationary solution is obtained by requiring the bracketed term to vanish, which leads to

$$3x - 8 = 1 \Rightarrow x = 3, \quad (39)$$

which is the KZ exponent for Case A with small n_κ at $\kappa \sim \beta$.

In Appendix D 4, we further provide a locality analysis which leads to a locality window of $5/2 < x < 4$. The solution $x = 3$ is therefore within the locality window and represents a valid local solution to the WKE.

2. Case B

Considering $n_3 \gg n_\kappa, n_1, n_2$ for I_1 and similar conditions for I_2 and I_3 , integrals (30)-(32) are reduced to

$$I_1 = \int \left| \frac{15\alpha^2}{128} \sqrt{\beta} \kappa \kappa_1 \kappa_2 \right|^2 n_\kappa n_1 n_2 n_3 \times \left[\frac{1}{n_\kappa} + \frac{1}{n_1} - \frac{1}{n_2} \right] \delta(\kappa + \kappa_1 - \kappa_2) d\kappa_1 d\kappa_2, \quad (40)$$

$$I_2 = \int \left| \frac{15\alpha^2}{128} \sqrt{\beta} \kappa \kappa_1 \kappa_3 \right|^2 n_\kappa n_1 n_2 n_3 \times \left[\frac{1}{n_\kappa} + \frac{1}{n_1} - \frac{1}{n_3} \right] \delta(\kappa + \kappa_1 - \kappa_3) d\kappa_1 d\kappa_3 \quad (41)$$

and

$$I_3 = \int \left| \frac{15\alpha^2}{128} \sqrt{\beta} \kappa \kappa_2 \kappa_3 \right|^2 n_\kappa n_1 n_2 n_3 \times \left[\frac{1}{n_\kappa} - \frac{1}{n_2} - \frac{1}{n_3} \right] \delta(\kappa - \kappa_2 - \kappa_3) d\kappa_2 d\kappa_3. \quad (42)$$

Defining

$$R_{12}^\kappa = \left| \frac{15\alpha^2}{128} \sqrt{\beta} \kappa \kappa_1 \kappa_2 \right|^2 n_\kappa n_1 n_2 n_3 \left[\frac{1}{n_\kappa} - \frac{1}{n_2} - \frac{1}{n_1} \right] \delta(\kappa - \kappa_2 - \kappa_1), \quad (43)$$

and applying the Zakharov transformations with the solution ansatz $n_\kappa \sim \kappa^{-x}$ (see Appendix D 3 for full details), we arrive at

$$I = \int R_{12}^\kappa \left[1 - \left(\frac{\kappa_1}{\kappa} \right)^{6x-8} - \left(\frac{\kappa_2}{\kappa} \right)^{6x-8} \right] d\kappa_1 d\kappa_2. \quad (44)$$

By enforcing the same condition as in §IIB 1, we find that the stationary solution is obtained at

$$6x - 8 = 1 \Rightarrow x = \frac{3}{2}, \quad (45)$$

which is the KZ exponent for Case B with large n_κ at $\kappa \sim \beta$. The locality analysis in Appendix D 4 shows a locality window of $4/3 < x < 5/2$, so that this KZ solution is local.

III. NUMERICAL STUDY

A subsequent numerical study is performed with the purpose of verifying the theoretical results derived in §II. In this section, we begin by outlining the methodology and numerical setup implemented in this study. We then discuss the results from two scenarios, namely, free-evolution and forced-dissipated configurations.

A. Methodology

We simulate the KB system (4) and (5) using a pseudospectral method paired with a fourth-order Runge-Kutta time marching scheme with an integration factor (IF-RK4) formulation [e.g., 34]. Key details of the

scheme can be found in Appendix F, along with a validation against existing exact solutions of the KB system. All numerical experiments are performed on a computational domain of size $L = 2\pi$ with periodic boundary conditions, discretized using $N = 4096$ free wave modes (before de-aliasing). The value of β is correspondingly chosen (and specified in each subsection) such that the high-order term in the dispersion relation in (8) is much smaller than the linear term, even for the highest wavenumber. In this section, we further present details of the numerical setup for the free-evolution and forced-dissipated cases in §III B 1 and §III B 2, respectively. We then introduce formulation of the direct scattering transform (DST), as well as the numerical strategies to solve the spectral problem for the purpose of testing isospectrality for the KB model associated with its integrability.

1. Free-evolution configuration

All freely evolving cases are performed without external forcing and damping, using a Gaussian spectrum $S(\kappa)$ as the initial condition [e.g., 23, 35]

$$S(\kappa) = Q \exp\left(-\frac{(\kappa - \kappa_p)^2}{2K^2}\right), \quad (46)$$

where $\kappa_p = 512$ represents the wavenumber peak, $K = 51.2$ characterizes the spectral bandwidth, and Q is chosen such that the resulting data size is $\lesssim 1$ (say measured by $\|\hat{\eta}_\kappa\|_\infty$ and $\|\hat{u}_\kappa\|_\infty$). The amplitude of each Fourier component $\hat{\eta}_\kappa$ is drawn from the spectrum $S(\kappa)$. To construct a bidirectional field, $\hat{\eta}_\kappa$ is evenly split to equally distribute energy between left- and right-propagating components. Each component is assigned a random phase drawn uniformly from $(0, 2\pi]$. The component \hat{u}_κ is then obtained from η_κ for both left- and right-propagating components via the linear relation. For all free-evolution experiments, we fix the dispersion parameter $\beta = 0.2$, and vary the nonlinearity parameter α to control the nonlinearity level.

2. Forced-dissipation configuration

All experiments begin from a quiescent initial state. Waves are excited by a forcing term $F(\kappa, t)$ added to the right-hand side of (5) (or (7) defined in the spectral domain), in the form of [e.g., 34, 36–38]

$$F(\kappa, t) = \begin{cases} f_\kappa \exp[-Ct + i(\omega_\kappa t + R)], & t \leq T_c, \\ f_\kappa \exp[-CT_c + i(\omega_\kappa t + R)], & t > T_c, \end{cases} \quad (47)$$

with

$$f_\kappa = \begin{cases} f_0 \frac{(\kappa - \kappa_1)(\kappa_2 - \kappa)}{(\kappa_1 - \kappa_2)^2}, & \kappa_1 \leq \kappa \leq \kappa_2, \\ 0, & \text{otherwise,} \end{cases} \quad (48)$$

where $f_0 = 0.88$ controls the forcing amplitude (leading to a solution of size $O(1)$ and mitigating the finite-size effect [e.g., 39–41]), $\kappa_1 = 26$ and $\kappa_2 = 38$ define the lower and upper bounds of the forcing band, and R is a uniformly distributed random number in the interval $(0, 2\pi]$. As defined in (47), the forcing amplitude decays exponentially at rate C for $t < T_c$ and remains constant for $t \geq T_c$. Such an implementation allows for a stationary state of the system to be achieved faster [37]. For this study, we set $T_c = 500T_p$ and $C = \ln 5/T_c$, where T_p is the peak period (computed using $\kappa_p = (\kappa_1 + \kappa_2)/2 = 32$).

To account for dissipation at small scales, we add terms $D_1 \hat{\eta}_\kappa$ and $D_1 \hat{u}_\kappa$ to (4) and (5), respectively. The dissipation coefficient takes the form [e.g., 36, 38]

$$D_1(\kappa) = \nu_1(\kappa - \kappa_{d1})^2, \quad \kappa \geq \kappa_{d1} \quad (49)$$

where $\nu_1 = 10^{-4}$ controls the dissipation strength, and $\kappa_{d1} = 900$ is the onset wavenumber. To distinguish Cases A and B, we introduce a hypo-viscous damping term at large scales only for Case A, with the coefficient in the form of

$$D_2(\kappa) = \nu_2 \kappa^{-4}, \quad \kappa \leq \kappa_{d2}. \quad (50)$$

where $\nu_2 = 5 \times 10^{-6}$. When (50) is applied, it introduces damping that suppresses n_κ at large scales, consistent with the assumption in Case A. Without this damping, the inverse cascade fills in large scales, causing n_κ to grow large in the simulation, consistent with Case B. In all forced-dissipated cases, we fix $\alpha = 0.0001$ and $\beta = 0.001$, so that the validity condition of normal form transformation is satisfied together with $O(1)$ solution size.

3. Direct scattering transform

In this study we utilize the direct scattering transform (DST) as a diagnostic tool. Since the KB system is completely integrable, it admits a Lax pair. We focus on the spectral problem alone, which suffices for the solution of DST. At each time instant, the spectral problem for the system is given by [3]

$$\Psi_{xx} + \left[k^2 + \frac{3}{4}\beta^{-1} + ikq(x) + r(x) \right] \Psi = 0 \quad (51)$$

where k is the eigenvalue, Ψ is the eigenfunction, and $q(x)$ and $r(x)$ are potentials defined as

$$q(x) = \frac{\sqrt{3}}{2} \alpha \beta^{-1/2} u(x), \quad r(x) = \frac{3}{4} \alpha \beta^{-1} \left(\eta(x) - \frac{1}{4} \alpha u(x)^2 \right),$$

which are assumed to decay to zero at $|x| \rightarrow \infty$. Solving the DST problem (51) amounts to finding the eigenvalue k and its corresponding eigenfunction Ψ . The property of the solution depends critically on the spectral parameter defined by $E(k) = \{k^2 + 3/(4\beta)\}^{1/2}$. However, $E(k)$ is a multivalued function in the complex plane of k , and

involves branch points at $k = \pm i\sqrt{3/(4\beta)}$ (more precisely, when a closed loop around $\pm i\sqrt{3/(4\beta)}$ is followed, $E(k)$ changes its value as the loop returns to the original point). Since it is inconvenient to work with a branch point, it is a conventional practice to perform a conformal transformation to the ζ -plane to eliminate these branch points [3]. The transformation is defined by

$$k = \frac{1}{4}(\zeta - \frac{B}{\zeta}), \quad E = \frac{1}{4}(\zeta + \frac{B}{\zeta})$$

with $B = 3/\beta$ so that $E(\zeta) = \{k(\zeta)^2 + 3/(4\beta)\}^{1/2}$ as defined above. The spectral problem (51) can now be written as

$$\Psi_{xx} + [E(\zeta)^2 + ik(\zeta)q(x) + r(x)]\Psi = 0, \quad (52)$$

where both k and E are single-valued in ζ . We have now circumvented the multivalued function and branch points that are associated with working in the k -plane. As a result, the transformation $\zeta \mapsto -B/\zeta$ changes the sign of E , $E \mapsto -E$, and leaves both k and E^2 invariant. Therefore, each ζ solution of (52) has a “mirror” part of $-B/\zeta$, and we plot in the result section only the one corresponding to the upper half E -plane, i.e., with $\text{Im}[E(\zeta)] > 0$ (see caption of Fig. 6 for details).

Referring to (52) again, we see that a continuous spectrum is characterized by $\text{Im}[E(\zeta)] = 0$, since at $|x| \rightarrow \infty$, it corresponds to an oscillatory solution of $\Psi(x)$. This solution occurs when ζ is either purely real or lies on the curve defined by $|\zeta| = \sqrt{3/\beta}$, as described in the caption of Fig. 2. We are interested in the discrete spectrum of eigenvalues that are away from the continuous spectrum, physically corresponding to bound states (or solitons).

The detailed numerical procedure to solve (52) is described in Appendix G. We further remark that the traditional DST procedure assumes the problem to be defined on \mathbb{R} , but our numerical solutions of $u(x)$ and $\eta(x)$ are periodic. For this reason, the DST may not be precise; nevertheless, it remains an effective tool for identifying bound states of the solution (see [42] for similar applications). In practice, this problem requires us to handle some spurious eigenvalues using a specific criterion detailed in Appendix G.

B. Results

1. Free-evolution experiments

We start by examining a free-evolution case with $\alpha = 0.2$ (and $\beta = 0.2$ for all cases in this section as presented in §III A 1), which corresponds to a traditional regime with dispersion balancing nonlinearity. We note that for $\alpha \sim \beta$, the validity condition of the normal form transformation is not satisfied, and the ensuing dynamics may be governed by quasi-resonant triad interactions. Figure 1 shows the evolution of the system from an initial Gaussian spectrum to the stationary spectrum evaluated

at $t = 2 \times 10^6 T_p$. It is clear that the wavenumber spectrum exhibits significant evolution, ultimately reaching a thermal-equilibrium state characterized by $n_\kappa \sim \kappa^{-1}$. Figure 2 presents the corresponding discrete eigenvalue spectrum obtained via the DST at the beginning and end of the simulation (we note that the identification of bound states in random wave background of high nonlinearity is also found in [42]). Aside from some very minor drift attributed to the periodic domain (in contrast to the unbounded domain \mathbb{R} assumed in theory), all eigenvalues remain essentially constant throughout the long-time evolution, consistent with the isospectral property of the integrable system. This case therefore provides strong evidence of the coexistence of integrability and wave kinetic behavior within the KB model.

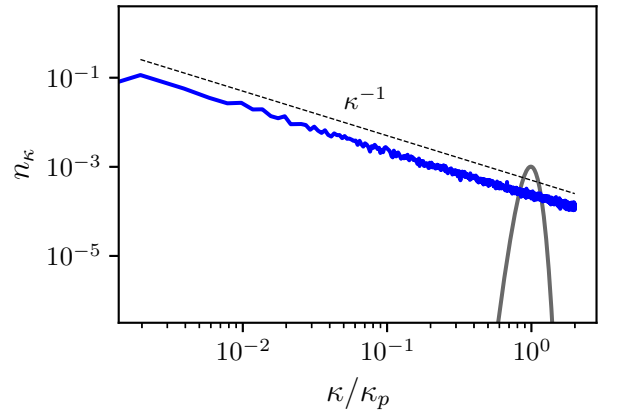


Figure 1. Initial (solid gray) and stationary (solid blue) spectra at $t = 0$ and $t = 2 \times 10^6 T_p$ for the free-evolution case with $\alpha = \beta = 0.2$. The thermal-equilibrium scaling is denoted (dashed black line).

We next study the spectral evolution for several values of α , in order to cover a broad range of nonlinearity associated with both triad and quartet interactions. Figure 3 shows the spectral evolution for $\alpha = 0.2, 0.04$ and 0.02 . We see that for all cases, the spectrum evolves into the same thermal-equilibrium state, although the corresponding evolution time differs (specifically, spectra are shown at $5 \times 10^5 T_p$, $8 \times 10^5 T_p$, and $1.2 \times 10^6 T_p$ for the three cases). The mechanisms driving thermalization, however, differ across cases. For sufficiently large values of α (i.e., those on the order of β), the dynamics are likely dominated by quasi-resonant triad interactions, as the normal form transformation is no longer theoretically applicable. As α decreases and enters the regime of $\alpha \ll \beta$, quartet interactions are expected to assume a more prominent role. To verify this hypothesis, in Appendix E, we present simulations of the KdV equation, which can be derived from the KB system by eliminating one direction of wave propagation. Since the KdV equation only supports waves travelling in a single direction, the resonance

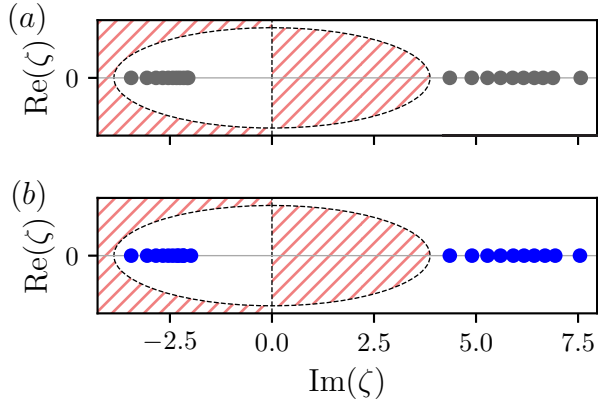


Figure 2. The spectrum of discrete eigenvalues ζ (blue and gray points) obtained via DST at (a) $t = 0$ and (b) $t \approx 2 \times 10^6 T_p$, corresponding to the times of initial and stationary spectra in Fig.1. The lower half E -plane (i.e., where $\text{Im}[E(\zeta)] < 0$) is marked by the red hashed region and the continuous spectrum region (i.e., where $\text{Im}[E(\zeta)] = 0$) is marked by the dashed black line.

condition for quartet interactions cannot be satisfied. For larger values of α (e.g., $\alpha = 0.2$), the KdV simulation exhibits thermalization on the same time scale as the KB simulation (similar thermalization behavior of KdV has also been observed in a previous numerical study [23]). In contrast, for smaller values of α (e.g., $\alpha = 0.02$), the KdV simulation is shown not to thermalize toward small scales due to the lack of quartet resonances. This differs from the KB simulation where quartet resonant interactions are critical for the same regime.

We further remark that the spectral evolution toward $n_\kappa \sim \kappa^{-1}$ is also observed in experiments of bidirectional shallow water waves, but it is often attributed to the soliton dynamics [e.g., 20–22]. To assess the influence of solitons in our study, we plot the wavenumber-frequency (k - ω) spectra from two representative simulations corresponding to the largest and smallest values of α in Fig. 4. We find that the energy branch in the k - ω spectra closely follows the free-wave dispersion relation (8), rather than the soliton dispersion relation marked in the figure. For the case with largest $\alpha = 0.2$, the soliton energy identified by the DST can be computed and found to only constitute 3% of the total energy, which is masked by the nonlinear broadening in Fig. 4(a). It is therefore safe to conclude that the thermalization observed in our study is caused by interactions among random free waves, rather than by soliton dynamics.

2. Forced-dissipated experiments

We now investigate the forced dissipated cases. In this section, we use $\alpha = 0.0001$ and $\beta = 0.001$, ensuring that

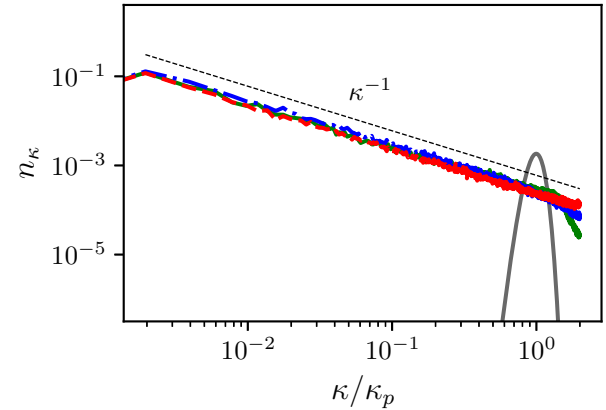


Figure 3. The initial spectrum (solid gray) and stationary spectra with $\alpha = 0.2$ (dashed red), $\alpha = 0.04$ (dashidot blue) and $\alpha = 0.02$ (solid green), respectively taken at $5 \times 10^5 T_p$, $8 \times 10^5 T_p$, and $1.2 \times 10^6 T_p$. The thermal-equilibrium scaling is denoted (dashed black).

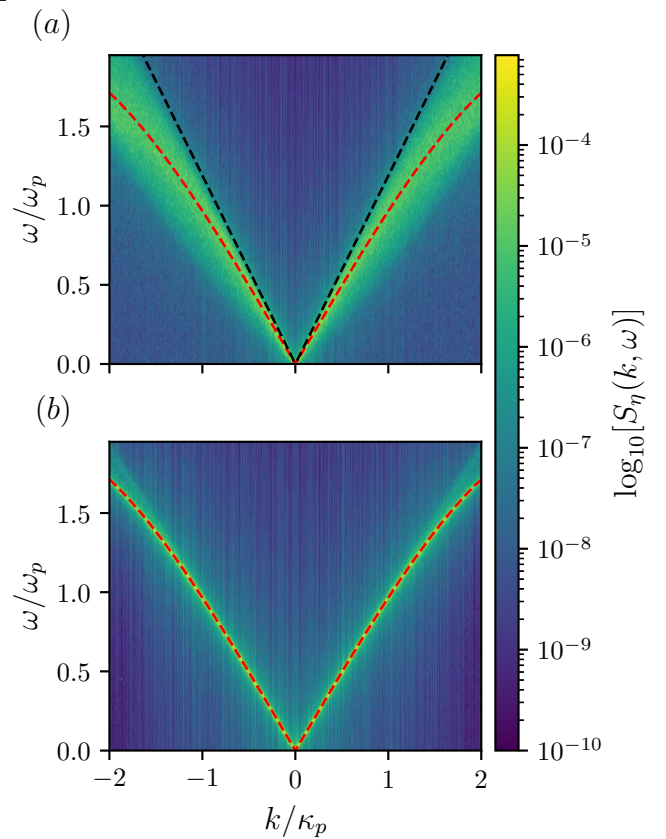


Figure 4. The k - ω spectra $S_\eta(k, \omega)$ for (a) $\alpha = 0.2$ and (b) $\alpha = 0.02$. The KB dispersion relation (8) is denoted by the dashed red line and the soliton dispersion relation (for the most dominant bound state) is denoted by the dashed black line in (a).

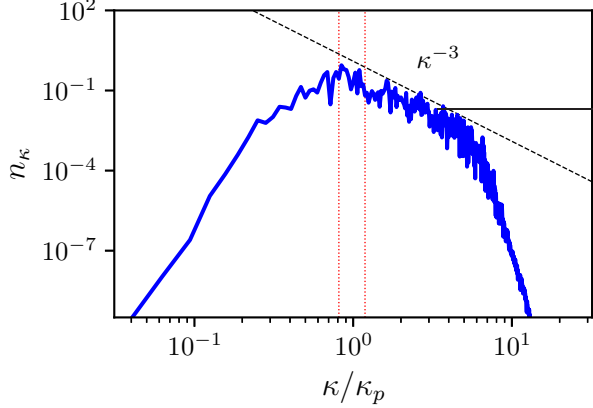


Figure 5. Stationary wave action spectrum for Case A. The forcing range is marked by the dotted red lines and the theoretical KZ scaling $n_\kappa \sim \kappa^{-3}$ is denoted by the dashed black line.

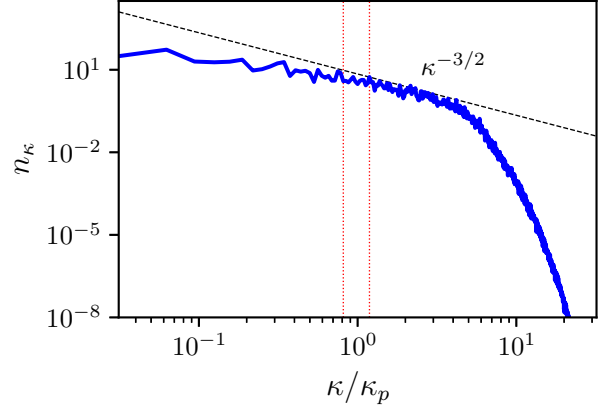


Figure 6. Stationary wave action spectrum for Case B. The forcing range is marked by the dotted red lines and the theoretical KZ scaling $n_\kappa \sim \kappa^{-3/2}$ is denoted by the dashed black line.

we operate in a regime where quartet interactions play a significant role in the spectral evolution toward small scales. We first present results with the presence of large-scale damping, corresponding to Case A in the theoretical derivation. Figure 5 shows the stationary spectrum after an evolution time of $6 \times 10^5 T_p$, where large scales contain minimal energy as desired. We see an inertial range slightly exceeding $2/3$ of a decade with a slope close to the theoretical prediction of κ^{-3} . Without large-scale damping, the resulting stationary spectrum corresponds to Case B with sufficiently high energy at large scales, as shown in Fig. 6. To the right of the forcing range, we see the formation of a $\kappa^{-3/2}$ spectrum spanning approximately $2/3$ of a decade, consistent with the theoretical prediction for Case B.

We remark that the results presented in this section differ substantially from the forced bidirectional shallow-water wave experiments in [20–22]. In these experiments, the system nonlinearity, measured by α/β , is high enough to induce the formation of a large number of solitons (i.e., soliton gas), which manifests itself as an exponentially decaying energy spectrum at moderate to small scales. In our study, α/β is kept low, suppressing the formation of solitons. This is confirmed by DST showing no bound state content in the system. Therefore, the observed power-law KZ scalings arise solely from interactions of free random waves.

IV. CONCLUSION AND DISCUSSION

In this work, we study the completely integrable (in the ISM sense) KB system and demonstrate non-trivial wave kinetics. A WKE is derived with a non-zero interaction coefficient on the four-wave resonant manifold, and the corresponding KZ solutions are obtained in a novel

way. In the derivation, we have also corrected several misconceptions regarding shallow-water wave turbulence, including the validity of the normal form transformation and the size of different terms in the interaction coefficient. The theoretical findings are verified by extensive numerical experiments, that directly demonstrate wave kinetic behavior including spectral thermalization and reproduction of KZ solutions under different conditions.

The emergence of non-trivial wave kinetics within an integrable framework challenges conventional views on the relationship between integrability and kinetic theory. Before discussing their general relation, it is important to highlight several features of the KB system that may be relevant here. First, the KB equation is mathematically ill-posed at high wavenumbers due to their exponential growth in time (see Eq. (8)). Although integrability theory (such as the formal construction of soliton solutions) remains applicable, the evolution problem itself is not well posed. To remedy this situation, one must impose an upper limit wavenumber cutoff k_{max} determined by the value of β , as done in our numerical simulations. This procedure, however, inevitably breaks the strict integrability of the system. If one takes $k_{max} \rightarrow \infty$, then one must set $\beta = 0$, for which $T_{k123} = 0$. However, in general, the integrability of the KB system holds for positive β , as used in this study.

Second, the spectral operator associated with the Lax pair of the KB system is non-self-adjoint. This property implies that the spectral problem admits complex eigenvalues, yielding possibly less stable spectral dynamics. This may induce instabilities that are responsible for the transfer of energy from low to high wavenumber modes. This process, which may be characterized by the growth of Sobolev norms, reflects the onset of wave kinetic behavior within the system.

Finally, we comment on the general relationship be-

tween integrability and kinetic theory. Integrable systems have been conventionally thought to yield trivial wave kinetics, most likely due to their limited phase space, which is constrained by conserved quantities. In the PDE setting, there is an infinite series of conserved quantities I_j , $j = 1, 2, \dots, \infty$ (or action variables in the action-angle formulation) on which the dynamics is trivial. However, it is possible that such trivial dynamics cannot be taken for granted for n_k , and to the authors' knowledge there is no proof associated with this issue. In general, I_j is connected to n_k through complicated nonlinear transformations, and trivial dynamics on one does not necessarily imply on the other. We believe that it is worthwhile to study the connection between I_j and n_k more thoroughly in future work across different integrable models, thereby providing a more elucidated understanding of the relation between integrability and kinetic theory.

Appendix A: Validity condition for the normal form transformation

We consider a spectrum (see Fig. 7) with finite bandwidth $\Delta = k^+ - k^-$, containing $N_\Delta = \Delta L/(2\pi)$ modes in Δ . We make the following assumptions:

1. the spectrum decays sufficiently fast outside $[k^-, k^+]$;
2. everything is comparable in the range $[k^-, k^+]$, i.e., $k^+ = C_1 k^-$, $\max(n(k)) = C_2 \min(n(k))$ for some constants C_1 and C_2 .

We note that assumption 1 is necessary to eliminate singularities arising from large wavenumbers in the normal form transformation, as elaborated later in this appendix.

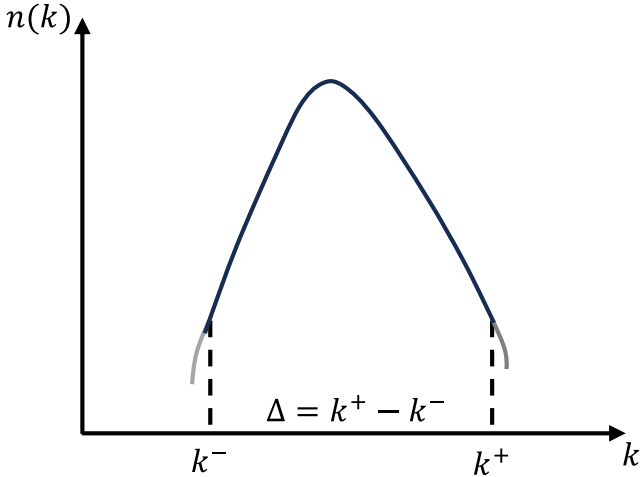


Figure 7. A sketch of the spectrum under consideration, with finite bandwidth Δ .

Our objective is to derive a condition under which (21) holds for $k \in p\mathbb{Z}$ where $p = 2\pi/L$. For this purpose, let

us consider the most singular terms on the left-hand side, i.e., those for which the denominators are of $O(\beta)$ rather than $O(1)$. For example, we take three wavenumbers in $\Gamma^{[1]}$ to be all positive, with $\omega_k - \omega_1 - \omega_2 \sim \beta k k_1 k_2$ in the first term and $\omega_k + \omega_1 - \omega_2 \sim \beta k k_1 k_2$ in the second term. Additionally, since $\omega_k + \omega_1 + \omega_2 \sim O(1)$ always holds, the third term can be neglected. Putting everything together, we have

$$\begin{aligned}
 \text{LHS} &\sim \left| \sum_{k_1+k_2=k, \text{all } >0} \frac{\alpha(k k_1 k_2)^{1/2}}{\beta k k_1 k_2} b_{k_1} b_{k_2} \right. \\
 &\quad \left. - 2 \sum_{k_1+k=k_2, \text{all } >0} \frac{\alpha(k k_1 k_2)^{1/2}}{\beta k k_1 k_2} b_{k_1}^* b_{k_2} \right| \\
 &\sim \left| \sum_{k_1=p}^{k-p} \frac{\alpha}{\beta[k k_1(k - k_1)]^{1/2}} b_{k_1} b_{k-k_1} \right. \\
 &\quad \left. + \sum_{k_1=p}^{\infty} \frac{\alpha}{\beta[k k_1(k + k_1)]^{1/2}} b_{k_1}^* b_{k+k_1} \right| \\
 &\sim \underbrace{\left| \sum_{k_1=p}^{k-p} \frac{\alpha}{\beta[k k_1(k - k_1)]^{1/2}} b_{k_1} b_{k-k_1} \right|}_{\textcircled{1}} \\
 &\quad + \underbrace{\sum_{k_1=p}^{k-p} \frac{\alpha}{\beta[k k_1(k + k_1)]^{1/2}} b_{k_1}^* b_{k+k_1}}_{\textcircled{2}} \\
 &\quad + \underbrace{\sum_{k_1=k}^{\infty} \frac{\alpha}{\beta[k k_1(k + k_1)]^{1/2}} b_{k_1}^* b_{k+k_1}}_{\textcircled{3}}.
 \end{aligned} \tag{A1}$$

In the above equation, it is evident that $\textcircled{1} > \textcircled{2}$ and

$$\begin{aligned}
 \textcircled{3} &< \sum_{k_1=k+p}^{\infty} \frac{\alpha}{\beta[k k_1|k - k_1|]^{1/2}} b_{k_1}^* b_{k+k_1} \\
 &\quad + \frac{\alpha}{\beta[k^2(k + k)]^{1/2}} b_k^* b_{2k} \\
 &\sim \sum_{k_1=k+p}^{\infty} \frac{\alpha}{\beta[k k_1|k - k_1|]^{1/2}} b_{k_1}^* b_{k+k_1}.
 \end{aligned}$$

Finally, we have

$$\text{LHS} \sim \left| \sum_{k_1=p, k_1 \neq k}^{\infty} \frac{\alpha}{\beta[k k_1|k - k_1|]^{1/2}} b_{k_1} b_{k-k_1} \right|. \tag{A2}$$

Here, we note that if $b_k \sim O(1)$ for all k , the summation in (A2) (or (A1)) does not converge at the ∞ end, as can be seen by replacing the summation by an integral. This problem is avoided with assumption 1 by introducing a

finite spectral bandwidth Δ . If one attempts to perform a more sophisticated analysis, the approach presented in [33] can be followed.

In further evaluating (A2), it is critical to take into account the random phases in b_k (a procedure not considered in [17]). More precisely, with random phases in b_k the summation on the left-hand side behaves like a random walk in the complex plane, for which cancellations due to walks in different directions must be considered. For this reason, the summation on the left-hand side should be evaluated in terms of the expected value $E[|\sum \cdot|]$ or $\{E[|\sum \cdot|^2]\}^{1/2}$. Taking the latter expression, we have

$$\begin{aligned} \text{LHS} &\sim \frac{\alpha}{\beta k^{1/2}} \left\{ E \left[\left| \sum_{k_1=p, k_1 \neq k}^{\infty} \frac{b_{k_1} b_{k-k_1}}{[k_1 |k - k_1|]^{1/2}} \right|^2 \right] \right\}^{1/2} \\ &\sim \frac{\alpha}{\beta k^{1/2}} \left\{ \sum_{k_1=p, k_1 \neq k}^{\infty} \frac{b_{k_1} b_{k-k_1}^* b_{k-k_1} b_{k-k_1}^*}{[k_1 |k - k_1|]} \right\}^{1/2} \\ &\sim \frac{\alpha |b_k|^2}{\beta k^{3/2}} \sqrt{N_{\Delta}} \ll |b_k|, \end{aligned} \quad (\text{A3})$$

where we have used Wick's pairing to obtain the second line, and assumptions 1 and 2 to obtain the third line.

We now estimate b_k using (11) and (18), which yields

$$|b_k| \sim |\eta_k|/k^{1/2} \sim \frac{1}{\sqrt{N_{\Delta} k^{1/2}}}, \quad (\text{A4})$$

where we have used $\sqrt{\sum_k |\eta_k|^2} \sim 1$ since the problem (e.g., significant wave height) has been scaled by a in (3).

Combining (A3) and (A4), we obtain $\alpha \ll \beta k^2$. If we further consider $k \sim 1$ (since the problem has been scaled by the peak wavenumber k_p), the condition is simply $\alpha \ll \beta$. Finally, we remark that the absence of N_{Δ} from the final result is only possible with the consideration of random phases in b_k .

Appendix B: Graphical proof regarding the resonant conditions

We consider the resonant condition

$$k_1 + k_2 = k_3 + k_4, \quad (\text{B1})$$

$$\omega_1 + \omega_2 = \omega_3 + \omega_4, \quad (\text{B2})$$

with a concave-down dispersion relation such as (8). A graphical illustration of the resonant condition is shown in Fig. 8. In general, there are two and only two types of solutions shown in the sub-figures (a) and (b). Figure 8(a) represents the solution with all wavenumbers positive. However, in this case, this solution corresponds to the trivial solution of $k_1 = k_4$ and $k_2 = k_3$, which

can be removed by a frequency renormalization in the four-wave dynamical equation. Figure 8(a) corresponds to the solution with one wavenumber (say k_4) negative and the other three positive. This solution is non-trivial and present in the WKE.

In summary, the only non-trivial solution for the resonant condition with a concave-down dispersion relation occurs when one wavenumber has an opposite sign with the other three.

Appendix C: Calculation regarding T_{I} and T_{II}

The interaction coefficient (20) consists of twelve terms, of which three belong to T_{I} and nine to T_{II} , according to (23). We begin by evaluating T_{I} , illustrating the procedure with the first term in (23). Substituting (17) into (23) yields

$$\begin{aligned} -\frac{V_{k,3,k-3} V_{2,1,2-1}}{\omega_1 + \omega_{2-1} - \omega_2} &= -\frac{\alpha^2 (\omega_k \omega_3 \omega_{k-3})^{1/2} (\omega_2 \omega_1 \omega_{2-1})^{1/2}}{32(\omega_1 + \omega_{2-1} - \omega_2)} \\ &\times [W_{k,3} + W_{k,k-3} + W_{3,k-3}] \\ &\times [W_{2,1} + W_{2,2-1} + W_{1,2-1}], \end{aligned} \quad (\text{C1})$$

where $W_{i,j} = W(i,j)$. We consider the condition corresponding to configuration 1, where k, k_1, k_2 are positive and k_3 is negative, with $\kappa_2 > \kappa, \kappa_1, \kappa_3$. The denominator of (C1) can be expanded using (8), yielding

$$\omega_1 + \omega_{2-1} - \omega_2 = \frac{1}{2} \beta \kappa \kappa_1 \kappa_2 (\kappa_2 - \kappa_1).$$

where the linear contribution from each term cancel and only $O(\beta)$ terms remain. Substituting this expression into (C1), and keeping only terms at leading order gives

$$-\frac{V_{k,3,k-3} V_{2,1,2-1}}{\omega_1 + \omega_{2-1} - \omega_2} = \frac{3\alpha^2}{16\beta} \left(\frac{\kappa_3 \kappa}{\kappa_1 \kappa_2} \right)^{1/2}. \quad (\text{C2})$$

Implementing the same procedure for the remaining T_{I} terms, we obtain

$$-\frac{V_{1,3,1-3} V_{2,k,2-k}}{\omega_k + \omega_{2-k} - \omega_2} = \frac{3\alpha^2}{16\beta} \left(\frac{\kappa_1 \kappa_3}{\kappa \kappa_2} \right)^{1/2}, \quad (\text{C3})$$

and

$$-\frac{V_{k+1,k,1} V_{2+3,2,3}}{\omega_{k+1} - \omega_k - \omega_1} = -\frac{3\alpha^2}{16\beta} \left(\frac{\kappa_3 \kappa_2}{\kappa \kappa_1} \right)^{1/2}. \quad (\text{C4})$$

By grouping (C2)-(C4) and using $\kappa_3 = \kappa_2 - \kappa - \kappa_1$, we can obtain a compact expression for T_{I}

$$T_{\text{I}} = -\frac{3\alpha^2}{16\beta} \left(\frac{\kappa_3^3}{\kappa \kappa_1 \kappa_2} \right)^{1/2}. \quad (\text{C5})$$

We next evaluate the contribution from the T_{II} terms in (23). The terms in T_{II} can be further subdivided into T_{II}^a

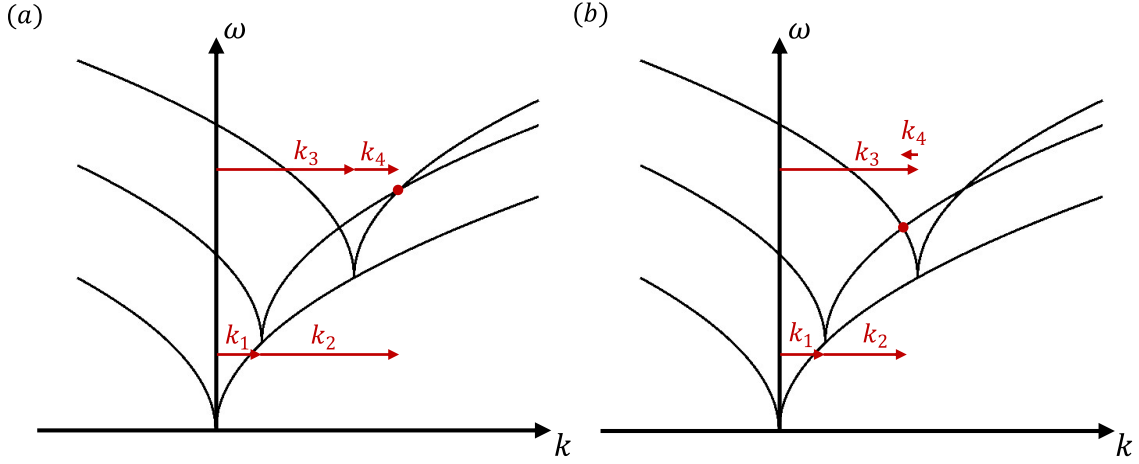


Figure 8. Graphical illustration of the resonant condition: (a) the case where all wavenumbers are positive; (b) the case where one wavenumber (say k_4) is negative and the others are positive.

and T_{II}^b based on how the linear terms in the denominator cancel—those with two linear terms after cancellation grouped into T_{II}^a , and those with one linear term grouped into T_{II}^b . Under this classification, T_{II}^a includes the first, third, and twelfth term in (20), and T_{II}^b includes the remaining terms. We begin with an example of calculation of one term in T_{II}^a , specifically taking the first term in (20),

$$-\frac{V_{k,2,k-2}V_{3,1,3-1}}{\omega_2 + \omega_{k-2} - \omega_k} = -\frac{\alpha^2(\omega_k\omega_2\omega_{k-2})^{1/2}(\omega_3\omega_1\omega_{3-1})^{1/2}}{32(\omega_2 + \omega_{k-2} - \omega_k)} \times [W_{k,2} + W_{k,k-2} + W_{2,k-2}] \times [W_{3,1} + W_{3,3-1} + W_{1,3-1}] \quad (C6)$$

Expanding the denominator and using $\omega_{k-2} = (\kappa_2 - \kappa) - \beta/6(\kappa_2 - \kappa)^3$ (due to configuration 1) gives

$$\omega_2 + \omega_{k-2} - \omega_k = -2(\kappa_2 - \kappa) - \frac{\beta}{6}[\kappa_2^3 + (\kappa_2 - \kappa)^3 - \kappa^3].$$

Substituting the expression above and only keeping terms at leading order into (C6), yields

$$-\frac{V_{k,2,k-2}V_{3,1,3-1}}{\omega_2 + \omega_{k-2} - \omega_k} = \frac{3\alpha^2}{64}(\kappa\kappa_1\kappa_2\kappa_3)^{1/2}, \quad (C7)$$

where the result is only one term after some cancellations. By repeating the same procedure for the remaining two T_{II}^a terms, one obtains

$$-\frac{V_{1,2,1-2}V_{3,k,3-k}}{\omega_2 + \omega_{1-2} - \omega_1} = \frac{3\alpha^2}{64}(\kappa\kappa_1\kappa_2\kappa_3)^{1/2} \quad (C8)$$

and

$$-\frac{V_{-k-1,k,1}V_{-2-3,2,3}}{\omega_{k+1} + \omega_k + \omega_1} = -\frac{3\alpha^2}{64}(\kappa\kappa_1\kappa_2\kappa_3)^{1/2}, \quad (C9)$$

. We next move onto terms belonging to T_{II}^b , using the second term in (20) as an example,

$$-\frac{V_{k,2,k-2}V_{3,1,3-1}}{\omega_1 + \omega_{3-1} - \omega_3} = -\frac{\alpha^2(\omega_k\omega_2\omega_{k-2})^{1/2}(\omega_3\omega_1\omega_{3-1})^{1/2}}{32(\omega_1 + \omega_{3-1} - \omega_3)} \times [W_{k,2} + W_{k,k-2} + W_{2,k-2}] \times [W_{3,1} + W_{3,3-1} + W_{1,3-1}] \quad (C10)$$

Expanding the denominator and using $\omega_{3-1} = (\kappa_3 + \kappa_1) - \beta/6(\kappa_3 + \kappa_1)^2$ (recall configuration 1) reveals that only one linear term remains

$$\omega_1 + \omega_{3-1} - \omega_3 = 2\kappa_1 - \frac{\beta}{6}[\kappa_1^3 + (\kappa_3 + \kappa_1)^3 - \kappa_3^3].$$

Substituting the above expression into (C10) and retaining only the leading-order contribution gives

$$-\frac{V_{k,2,k-2}V_{3,1,3-1}}{\omega_1 + \omega_{3-1} - \omega_3} = \frac{3\alpha^2\kappa_3(\kappa\kappa_1\kappa_2\kappa_3)^{1/2}}{64\kappa_1} + \frac{3\alpha^2}{64}(\kappa\kappa_1\kappa_2\kappa_3)^{1/2}. \quad (C11)$$

Carrying out the same calculation for the five remaining T_{II}^b gives

$$-\frac{V_{1,2,1-2}V_{3,k,3-k}}{\omega_k + \omega_{3-k} - \omega_3} = \frac{3\alpha^2\kappa_3(\kappa\kappa_1\kappa_2\kappa_3)^{1/2}}{64\kappa} + \frac{3\alpha^2}{64}(\kappa\kappa_1\kappa_2\kappa_3)^{1/2}, \quad (C12)$$

$$-\frac{V_{k,3,k-3}V_{2,1,2-1}}{\omega_3 + \omega_{k-3} - \omega_k} = \frac{3\alpha^2\kappa(\kappa\kappa_1\kappa_2\kappa_3)^{1/2}}{64\kappa_3} + \frac{3\alpha^2}{64}(\kappa\kappa_1\kappa_2\kappa_3)^{1/2}, \quad (C13)$$

$$-\frac{V_{1,3,1-3}V_{2,k,2-k}}{\omega_3 + \omega_{1-3} - \omega_1} = \frac{3\alpha^2\kappa_1(\kappa\kappa_1\kappa_2\kappa_3)^{1/2}}{64\kappa_3} + \frac{3\alpha^2}{64}(\kappa\kappa_1\kappa_2\kappa_3)^{1/2}, \quad (\text{C14})$$

$$-\frac{V_{k+1,k,1}V_{2+3,2,3}}{\omega_{2+3} - \omega_2 - \omega_3} = \frac{3\alpha^2}{64}(\kappa\kappa_1\kappa_2\kappa_3)^{1/2} - \frac{3\alpha^2\kappa_2(\kappa\kappa_1\kappa_2\kappa_3)^{1/2}}{64\kappa_3}, \quad (\text{C15})$$

and

$$-\frac{V_{-k-1,k,1}V_{-2-3,2,3}}{\omega_{2+3} + \omega_2 + \omega_3} = \frac{3\alpha^2}{64}(\kappa\kappa_1\kappa_2\kappa_3)^{1/2} - \frac{3\alpha^2\kappa_3(\kappa\kappa_1\kappa_2\kappa_3)^{1/2}}{64\kappa_2}. \quad (\text{C16})$$

Grouping terms (C7)-(C9) for T_{II}^a and (C11)-(C16) for T_{II}^b and using the relation $\kappa_3 = \kappa_2 - \kappa - \kappa_1$ yields

$$T_{\text{II}}^a = \frac{3\alpha^2}{64}(\kappa\kappa_1\kappa_2\kappa_3)^{1/2} \quad (\text{C17})$$

$$T_{\text{II}}^b = \frac{3\alpha^2}{64}(\kappa\kappa_1\kappa_2\kappa_3)^{1/2} \left[\kappa_3 \left(\frac{1}{\kappa_1} + \frac{1}{\kappa} - \frac{1}{\kappa_2} \right) + 5 \right].$$

Combining T_{II}^a and T_{II}^b yields the compact expression

$$T_{\text{II}} = \frac{3\alpha^2}{64}(\kappa\kappa_1\kappa_2\kappa_3)^{1/2} \left[\kappa_3 \left(\frac{1}{\kappa_1} + \frac{1}{\kappa} - \frac{1}{\kappa_2} \right) + 6 \right]. \quad (\text{C18})$$

(C5) and (C18) are given by (24) in §II A of the main paper. To obtain the correct β dependence of T_{I} and T_{II} , we need to further substitute the expression for κ_3 (i.e., (D2) in Appendix II B) into (C5) and (C18),

$$T_{\text{I}} = -\frac{3\alpha^2}{128}\beta^{1/2}\kappa\kappa_1\kappa_2, \quad (\text{C19})$$

$$T_{\text{II}} = \frac{9\alpha^2}{64}\beta^{1/2}\kappa\kappa_1\kappa_2 - \frac{3\alpha^2}{512}\beta^{3/2}\kappa\kappa_1\kappa_2(\kappa\kappa_1 - \kappa_2\kappa_1 - \kappa\kappa_2).$$

For small β , the $\beta^{3/2}$ term in T_{II} can be neglected, allowing us to express the total coefficient in a compact form

$$T_{k123} = T_{\text{I}} + T_{\text{II}} = \frac{15\alpha^2}{128}\beta^{1/2}\kappa\kappa_1\kappa_2. \quad (\text{C20})$$

Appendix D: Details of KZ spectra derivation

1. Reduction of resonance condition in I -terms

We begin by using I_1 as an example. To impose the resonant constraint, we substitute the wavenumber resonance condition $\kappa_3 = -\kappa - \kappa_1 + \kappa_2$ into the frequency resonance condition using (8), which gives

$$\omega_\kappa + \omega_1 - \omega_2 - \omega_3 = -2\kappa_3 - \frac{\beta}{6}(\kappa^3 + \kappa_1^3 - \kappa_2^3 - \kappa_3^3) = 0.$$

For a non-trivial solution, κ_3 must be of $O(\beta)$. As a result, $\kappa_3^3 = O(\beta^3)$ is negligible at leading order and can be omitted, yielding

$$\kappa_3 = \frac{\beta}{12}(\kappa_2^3 - \kappa^3 - \kappa_1^3). \quad (\text{D1})$$

The argument of the wavenumber delta function may be written as

$$\kappa + \kappa_1 - \kappa_2 + O(\beta) = 0,$$

since it is appropriate to neglect the $O(\beta)$ term at leading order. This new resonant condition implies $\kappa_2 = \kappa + \kappa_1$, which simplifies (D1) to

$$\kappa_3 = \frac{\beta}{4}\kappa\kappa_1\kappa_2. \quad (\text{D2})$$

Following a similar procedure, we obtain the relations $\kappa_2 = (\beta/4)\kappa\kappa_1\kappa_3$ and $\kappa_1 = (\beta/4)\kappa\kappa_2\kappa_3$ corresponding to I_2 and I_3 respectively. Substituting these $\kappa_i \sim \beta$ terms into the interaction coefficient (27) and integrating out the frequency condition in each case yields (30)-(32) presented in the main paper.

2. Case A

We seek stationary power-law solutions of the form $n_\kappa \sim \kappa^{-x}$. The total interaction is given by (37) in the main paper, with the kernel R_{12}^κ defined by (36). We adopt the reference form $R_{12}^\kappa \propto (\kappa\kappa_1\kappa_2)^{2-x}\delta(\kappa - \kappa_2 - \kappa_1)$ and rewrite the other two permutations, $R_{1\kappa}^2$ and $R_{\kappa 2}^1$, into this form via Zakharov transformations (ZT) as introduced in [1]. Inserting the power-law solution ansatz and performing the ZT on $R_{1\kappa}^2$ using $\kappa_1 = \kappa^2/\tilde{\kappa}_1$ and $\kappa_2 = \kappa\tilde{\kappa}_2/\tilde{\kappa}_1$ with Jacobian $|\kappa^3/\tilde{\kappa}_1^3|$ yields

$$R_{1\kappa}^2 d\kappa_1 d\kappa_2 \propto (\kappa^{10-4x}\tilde{\kappa}_1^{2x-6}\tilde{\kappa}_2^{2x-6})\delta(\kappa - \tilde{\kappa}_2 - \tilde{\kappa}_1)d\tilde{\kappa}_1 d\tilde{\kappa}_2.$$

From this, the integral contribution relative to the reference kernel becomes

$$I_2 = \int \left(\frac{\kappa_1}{\kappa} \right)^{3x-8} R_{12}^\kappa d\kappa_1 d\kappa_2,$$

which serves as a key component for determining the stationary scaling exponent.

Following the same procedure for $R_{\kappa 2}^1$ with $\kappa_1 = \kappa\tilde{\kappa}_1/\tilde{\kappa}_2$, $\kappa_2 = \kappa^2/\tilde{\kappa}_2$ and Jacobian $|\kappa^3/\tilde{\kappa}_2^3|$ yields

$$R_{\kappa 2}^1 d\kappa_1 d\kappa_2 \propto (\kappa^{10-4x}\tilde{\kappa}_1^{2x-6}\tilde{\kappa}_2^{2x-6})\delta(\kappa - \tilde{\kappa}_2 - \tilde{\kappa}_1)d\tilde{\kappa}_1 d\tilde{\kappa}_2,$$

which in turn yield

$$I_3 = \int \left(\frac{\kappa_2}{\kappa} \right)^{3x-8} R_{12}^\kappa d\kappa_1 d\kappa_2.$$

The total contribution can then be written as

$$I = \int R_{12}^\kappa \left[1 - \left(\frac{\kappa_1}{\kappa} \right)^{3x-8} - \left(\frac{\kappa_2}{\kappa} \right)^{3x-8} \right] d\kappa_1 d\kappa_2,$$

which is presented as (38) in the main paper.

3. Case B

Here we consider the solution ansatz $n_\kappa \sim \kappa^{-x}$ and take $R_{12}^\kappa \propto \kappa^{2-2x} \kappa_1^{2-2x} \kappa_2^{2-2x}$ (from (43) in the main paper) as the reference form. Applying the same ZT outlined in §D 2 to $R_{1\kappa}^2$ yields

$$R_{1\kappa}^2 d\kappa_1 d\kappa_2 = 4^x \beta^{-x} (\kappa^{10-8x} \tilde{\kappa}_1^{4x-6} \tilde{\kappa}_2^{2-2x}) \times \delta(\kappa - \tilde{\kappa}_2 - \tilde{\kappa}_1) d\tilde{\kappa}_1 d\tilde{\kappa}_2.$$

Consequently, the integral contribution relative to the reference kernel is

$$I_2 = \int \left(\frac{\kappa_1}{\kappa} \right)^{6x-8} R_{12}^\kappa d\kappa_1 d\kappa_2.$$

Applying the same procedure to $R_{\kappa 2}^1$ using the transformations outlined in §D 2 gives the following

$$R_{\kappa 2}^1 d\kappa_1 d\kappa_2 = 4^x \beta^{-x} (\kappa^{10-8x} \tilde{\kappa}_1^{2-2x} \tilde{\kappa}_2^{4x-6}) \times \delta(\kappa - \tilde{\kappa}_2 - \tilde{\kappa}_1) d\tilde{\kappa}_1 d\tilde{\kappa}_2,$$

which yields

$$I_3 = \left(\frac{\kappa_2}{\kappa} \right)^{6x-8} R_{12}^\kappa d\kappa_1 d\kappa_2.$$

The total interaction term can therefore be written as

$$I = \int R_{12}^\kappa \left[1 - \left(\frac{\kappa_1}{\kappa} \right)^{6x-8} - \left(\frac{\kappa_2}{\kappa} \right)^{6x-8} \right] d\kappa_1 d\kappa_2,$$

which corresponds to (44) in the main paper.

4. Locality of solutions

We analyze the locality of the spectrum $n_\kappa \sim \kappa^{-x}$ by evaluating the behavior in the infrared (IR) and ultraviolet (UV) limits.

We begin by assessing the behavior in the IR limit for Case A. To this end, we take $\kappa_1 \rightarrow 0$. Expressing the interaction term R_{12}^κ given by (36) in terms of the power-law ansatz yields

$$R_{12}^\kappa \propto (\kappa \kappa_1 \kappa_2)^2 (\kappa^{-x} \kappa_1^{-x} \kappa_2^{-x}) \delta(\kappa - \kappa_2 - \kappa_1). \quad (\text{D3})$$

Integrating out κ_2 we obtain

$$R^a(\kappa, \kappa_1) \propto \kappa^{2-x} \kappa_1^{2-x} (\kappa - \kappa_1)^{2-x} \quad (\text{D4})$$

Expanding the $(\kappa - \kappa_1)^{2-x}$ term in (D4) leads to

$$(\kappa - \kappa_1)^{2-x} \approx \kappa^{2-x} - (2-x) \kappa^{1-x} \kappa_1 + \dots,$$

which can then be substituted back into (D4) yielding

$$R^a(\kappa, \kappa_1) \propto \kappa_1^{2-x} \kappa^{4-2x} - (2-x) \kappa^{3-2x} \kappa_1^{3-x}. \quad (\text{D5})$$

Following the same procedure for $R_{1\kappa}^2$, we obtain

$$R^b(\kappa, \kappa_1) \propto \kappa_1^{2-x} \kappa^{4-2x} + (2-x) \kappa^{3-2x} \kappa_1^{3-x}. \quad (\text{D6})$$

In the case of $R_{\kappa 2}^1$, taking $\kappa_1 \rightarrow 0$ while κ as $O(1)$ means that the resonance condition cannot be satisfied, therefore $R^c(\kappa, \kappa_1) = 0$. From the total interaction integral

$$I(\kappa) = \int (R^a - R^b - R^c) d\kappa_1 \sim \int \kappa_1^{3-x} d\kappa_1, \quad (\text{D7})$$

where we see that (D5) and (D6) cancel at the leading order. For the integral (D7) to converge, we require $3 - x > -1$, resulting in the condition

$$\text{IR convergence (A): } x < 4. \quad (\text{D8})$$

Next, we assess the behavior in the UV limit for Case A by taking $\kappa_1 \rightarrow \infty$. For R_{12}^κ , the resonance condition cannot be satisfied when taking $\kappa_1 \rightarrow \infty$, thus it does not contribute (i.e., $R^a(\kappa, \kappa_1) = 0$). For the next term with the solution ansatz

$$R_{1\kappa}^2 \propto (\kappa \kappa_1 \kappa_2)^2 (\kappa^{-x} \kappa_1^{-x} \kappa_2^{-x}) \delta(\kappa_2 - \kappa - \kappa_1). \quad (\text{D9})$$

Integrating out κ_2 yields

$$R^b(\kappa, \kappa_1) \propto \kappa^{2-x} \kappa_1^{2-x} (\kappa_1 + \kappa)^{2-x} \quad (\text{D10})$$

which, upon substitution of the expansion $(\kappa_1 + \kappa)^{2-x} \approx \kappa_1^{2-x} + (2-x) \kappa_1^{1-x} \kappa_1 + \dots$ yields

$$R^b(\kappa, \kappa_1) \propto \kappa^{2-x} \kappa_1^{4-2x} - (2-x) \kappa^{3-x} \kappa_1^{3-2x}. \quad (\text{D11})$$

Following the the same procedure for $R^1 \kappa 2$ gives

$$R^c(\kappa, \kappa_1) \propto \kappa^{2-x} \kappa_1^{4-2x} + (2-x) \kappa^{3-x} \kappa_1^{3-2x}. \quad (\text{D12})$$

Explicitly evaluating $R^a - R^b - R^c$ reveals the following scaling in the UV limit

$$I(\kappa) \sim \int \kappa_1^{4-2x} d\kappa_1. \quad (\text{D13})$$

Convergence of (D13) therefore requires $4 - 2x < -1$, yielding the criterion

$$\text{UV convergence (A): } x > 5/2. \quad (\text{D14})$$

We next assess the behavior in the IR limit for Case B by making $\kappa_1 \rightarrow 0$. If we express (43) in terms of the power-law ansatz $n_\kappa \sim \kappa^{-x}$, we obtain

$$R_{12}^\kappa \propto (\kappa \kappa_1 \kappa_2)^2 (\kappa^{-x} \kappa_1^{-x} \kappa_2^{-x} \kappa_3^{-x}) (\kappa^x - \kappa_1^x - \kappa_2^x) \times \delta(\kappa - \kappa_2 - \kappa_1). \quad (\text{D15})$$

Using $\kappa_3 = (\beta/4) \kappa_1 \kappa_2 \kappa_2$ from (D2), we can simplify (D15) to

$$R_{12}^\kappa \propto (\kappa \kappa_1 \kappa_2)^{2-2x} (\kappa^x - \kappa_1^x - \kappa_2^x) \delta(\kappa - \kappa_1 - \kappa_2). \quad (\text{D16})$$

Integrating out κ_2 gives

$$R^a(\kappa, \kappa_1) \propto (\kappa\kappa_1(\kappa - \kappa_1))^{2-2x} (\kappa^x + \kappa_1^x - (\kappa - \kappa_1)^x), \quad (\text{D17})$$

which upon substituting the expansion of $(\kappa - \kappa_1)^x$ and $(\kappa - \kappa_1)^{2-2x}$ yields

$$R^a(\kappa, \kappa_1) \propto x\kappa^{3-3x}\kappa_1^{3-2x} - (2-2x)x\kappa^{2-3x}\kappa_1^{4-2x}. \quad (\text{D18})$$

Following the same procedure for $R_{1\kappa}^2$ gives

$$R^b(\kappa, \kappa_1) \propto x\kappa^{3-3x}\kappa_1^{3-2x} + (2-2x)x\kappa^{2-3x}\kappa_1^{4-2x}. \quad (\text{D19})$$

As stated in Case A, $R_{\kappa 2}^1$ does not contribute when $\kappa_1 \rightarrow 0$, therefore $R^c(\kappa, \kappa_1) = 0$. Explicitly evaluating $R^a - R^b - R^c$ shows that the leading-order terms of (D18) and (D19) cancel. Thus, the integral in the IR limit behaves like

$$I(\kappa) \sim \int \kappa_1^{4-2x} d\kappa_1 \quad (\text{D20})$$

For (D20) to converge, the exponent must satisfy $4-2x > -1$, which yields the condition

$$\text{IR convergence (B): } x < 5/2. \quad (\text{D21})$$

Next we take $\kappa_1 \rightarrow \infty$ to assess behavior in the UV limit. In this scenario, $R_{12}^\kappa = 0$ (and thus $R^a(\kappa, \kappa_1) = 0$) for the same reason stated above for Case A. The interaction term $R_{1\kappa}^2$ can be expressed as

$$R_{1\kappa}^2 \propto (\kappa\kappa_1\kappa_2)^{2-2x} (\kappa_2^x - \kappa^x - \kappa_1^x) \delta(\kappa_2 - \kappa - \kappa_1). \quad (\text{D22})$$

After integrating out κ_2 we get

$$R^b(\kappa, \kappa_1) \propto (\kappa\kappa_1(\kappa_1 + \kappa))^{2-2x} (\kappa^x + \kappa_1^x - (\kappa_1 + \kappa)^x), \quad (\text{D23})$$

into which we substitute the expansion for $(\kappa_1 + \kappa)^{2-2x}$ and $(\kappa_1 + \kappa)^x$ yielding

$$R^b(\kappa, \kappa_1) \propto (2x - 2x^2)\kappa^{4-2x}\kappa_1^{3-2x} + x\kappa^{3-2x}\kappa_1^{3-3x}. \quad (\text{D24})$$

Carrying out the same procedure on $R_{2\kappa}^1$ gives

$$R^c(\kappa, \kappa_1) \propto -(2x - 2x^2)\kappa^{4-2x}\kappa_1^{3-2x} + x\kappa^{3-2x}\kappa_1^{3-3x}. \quad (\text{D25})$$

Evaluating $R^a - R^b - R^c$ shows that the first terms in (D24) and (D25) cancel, and the integral scales as

$$I(\kappa) \sim \int \kappa_1^{3-3x} d\kappa_1 \quad (\text{D26})$$

In order for the integral to converge, we require $3-3x < -1$, leading to the condition

$$\text{UV convergence (B): } x > 4/3. \quad (\text{D27})$$

Appendix E: Unidirectional KdV simulations

Following the procedure outlined in [43] (see Ch. 3), a KdV equation can be derived from the KB system (1) and (2) by eliminating one direction of wave propagation. The KdV equation reads

$$\eta_t + \eta_x + \frac{3}{2}\alpha\eta\eta_x + \frac{1}{6}\beta\eta_{xxx} = 0. \quad (\text{E1})$$

We perform numerical simulations of (E1) using a pseudospectral method combined with an IF-RK4 time-marching scheme. The computational setup follows the configuration detailed in §III A 1, with the sole modification that the initial condition now only contains right-propagating waves. Figure 9(a) compares the spectral evolution of the KdV equation and the KB system for $\alpha = \beta = 0.2$. Both spectra reach the same thermal-equilibrium form on the same time scale, with the respective spectra evaluated at $t = 5 \times 10^5 T_p$. This behavior is to be expected, as when nonlinearity and dispersion are balanced, the dynamics are primarily governed by quasi-resonant interaction, which are supported in both KB and KdV frameworks.

In contrast, Fig. 9(b) presents the spectral evolution for $\alpha = 0.02$ in the regime $\alpha \ll \beta$, where a clear disparity emerges between the dynamics of the KdV equation and the KB system. We see that the spectrum from the KB equation thermalizes at all scales, but the spectrum from the KdV equation only thermalizes at large scales. We recall that in this regime of $\alpha \ll \beta$, the normal form transformation is valid and the quartet interactions play a significant role in the spectral evolution. This is indeed the mechanism driving thermalization of the KB spectrum toward moderate-to-small scales, which on the other hand is absent in the KdV system. We further note that the validity condition of the normal form transformation requires the spectrum to decay sufficiently fast at large scales, which is not the case as in the simulations (more precisely, the validity condition should read $\alpha \ll \beta k^2$ which is not satisfied at small k). Therefore, the evolution of large scales may still be driven by triad quasi-resonances in both the KB and KdV simulations, as we observe in Fig. 9(b).

Appendix F: Numerical scheme and validation

1. Time Integration Scheme

In this appendix we describe the IF-RK4 scheme for the KB system. We start by splitting the linear and nonlinear parts of equations (4) and (5) and expressing them in Fourier space (essentially following the procedure in [34]):

$$\frac{\partial}{\partial t} \begin{bmatrix} \hat{\eta}_k \\ \hat{u}_k \end{bmatrix} = ik \begin{bmatrix} 0 & -1 + \frac{\beta}{3}k^2 \\ -1 & 0 \end{bmatrix} \begin{bmatrix} \hat{\eta}_k \\ \hat{u}_k \end{bmatrix} + \begin{bmatrix} \hat{P}_k \\ \hat{Q}_k \end{bmatrix} \quad (\text{F1})$$

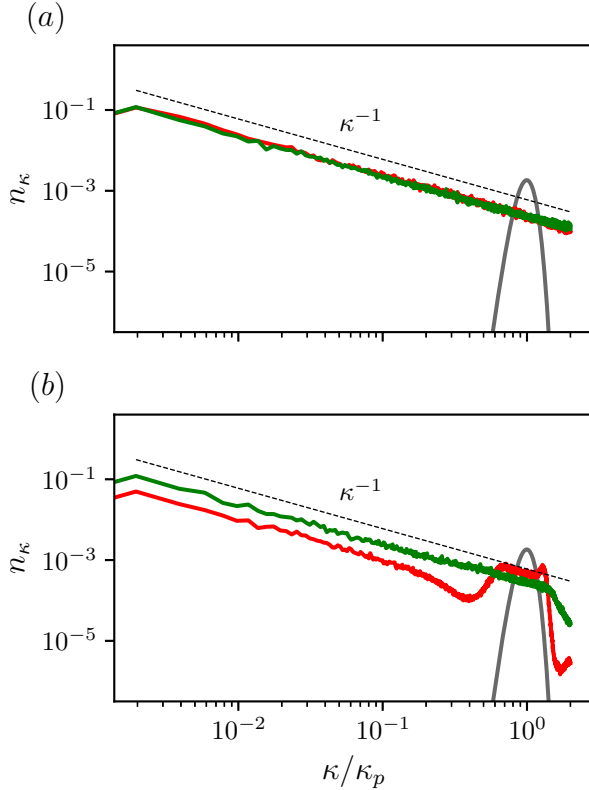


Figure 9. The spectrum $n_k \propto |\eta_k|^2/\omega_k$ at the initial (solid gray) and stationary state for KB (solid green) and KdV (red) for (a) $\alpha = 0.2$ taken at $5 \times 10^5 T_p$ and (b) $\alpha = 0.02$ taken at $1.2 \times 10^6 T_p$. The thermal-equilibrium scaling is denoted (dashed black).

where $\hat{\eta}_k$ and \hat{u}_k are the Fourier transforms of $\eta(x)$ and $u(x)$, and \hat{P}_k and \hat{Q}_k represent the nonlinear terms in (4) and (5). Diagonalizing (F1) yields

$$\frac{\partial}{\partial t} \begin{bmatrix} v_1 \\ v_2 \end{bmatrix} = ik \begin{bmatrix} \lambda_1 & 0 \\ 0 & \lambda_2 \end{bmatrix} \begin{bmatrix} v_1 \\ v_2 \end{bmatrix} + \begin{bmatrix} F_1 \\ F_2 \end{bmatrix} \quad (\text{F2})$$

where $\lambda_1 = -ik\sqrt{1 - \frac{\beta}{3}k^2}$ and $\lambda_2 = ik\sqrt{1 - \frac{\beta}{3}k^2}$, and

$$\begin{bmatrix} v_1 \\ v_2 \end{bmatrix} = \Omega^{-1} \begin{bmatrix} \hat{\eta}_k \\ \hat{u}_k \end{bmatrix}, \quad (\text{F3})$$

$$\begin{bmatrix} F_1 \\ F_2 \end{bmatrix} = \Omega^{-1} \begin{bmatrix} \hat{P}_k \\ \hat{Q}_k \end{bmatrix}, \quad (\text{F4})$$

with

$$\Omega = \begin{bmatrix} \sqrt{1 - \frac{\beta}{3}k^2} & -\sqrt{1 - \frac{\beta}{3}k^2} \\ 1 & 1 \end{bmatrix}. \quad (\text{F5})$$

We then define $\Psi_1 = \exp(-\lambda_1 t)v_1$ and $\Psi_2 = \exp(-\lambda_2 t)v_2$, with which (F2) can be transformed into

$$\frac{\partial}{\partial t} \Psi_1 = \exp(-\lambda_1 t)F_1, \quad (\text{F6})$$

$$\frac{\partial}{\partial t} \Psi_2 = \exp(-\lambda_2 t)F_2. \quad (\text{F7})$$

Equations (F6) and (F7) can then be integrated using the standard RK4 scheme. This combined IF-RK4 scheme essentially solves the linear part of (F2) analytically (to machine precision, see Fig. 10 for validation). A similar scheme is implemented for simulations of the KdV equation. An integrating factor can be applied directly to the KdV equation [44], in contrast to the coupled KB system which must first be diagonalized.

For both KB and KdV, the spatial derivatives, including the nonlinear terms \hat{P}_k and \hat{Q}_k in the former, are computed using Fast Fourier Transforms. To mitigate aliasing errors, we use a 1/2 de-aliasing rule.

2. Validation of KB System

We perform a series of tests to validate the aforementioned methods. We begin by ensuring that the linear part of the KB system is solved to machine precision using the integrating factor scheme. To do this, we set $\alpha = 0$, discarding the nonlinear terms in (4) and (5), we are left with:

$$\eta_t = -u_x - \frac{1}{3}\beta u_{xxx}, \quad (\text{F8})$$

$$u_t = -\eta_x. \quad (\text{F9})$$

This system has an exact solution of the form $\sin(kx - \omega t)$. Substituting this in for u , we get:

$$\begin{aligned} u(x, t) &= \sin(kx - \omega t) \\ \eta(x, t) &= \frac{\omega}{k} \sin(kx - \omega t) \end{aligned} \quad (\text{F10})$$

where the dispersion relation is given by (8). For this test case, we set $\beta = 1$ and use (F10) as our initial condition with $t = 0$. Figure 10 shows the numerical solution compared against the analytic solution after $10T_p$. Both the velocity component and the surface elevation are within machine precision of the analytic solution.

We proceed with the full KB system where we set $\alpha = \beta = 1$. The solver is tested using a known exact soliton solution (example taken from [45])

$$\begin{aligned} u(x, t) &= \frac{2(c^2 - 1)}{\cosh(\sqrt{3(c^2 - 1)}(x - ct)) + c} \\ \eta(x, t) &= cu(x, t) - \frac{1}{2}u^2(x, t) \end{aligned} \quad (\text{F11})$$

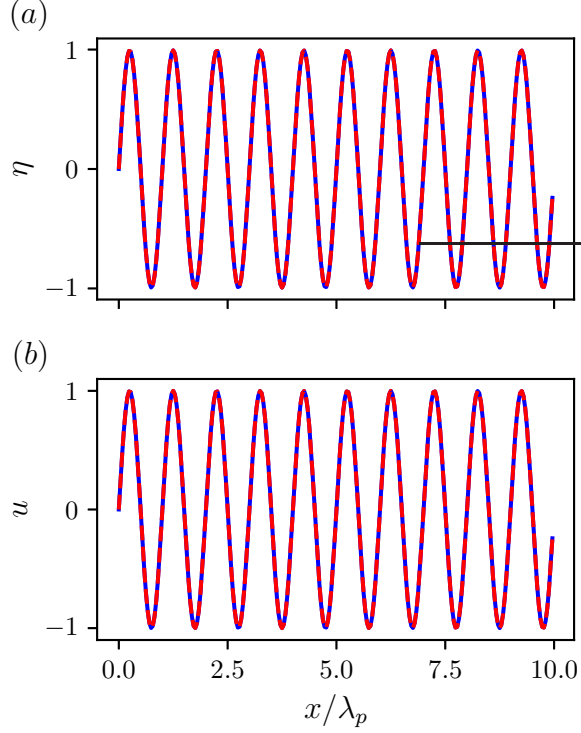


Figure 10. Comparison of the numerical (solid blue) and analytical (dashed red) solutions for (a) velocity and (b) surface elevation for the linear portion of the KB system at $t = 10T_p$.

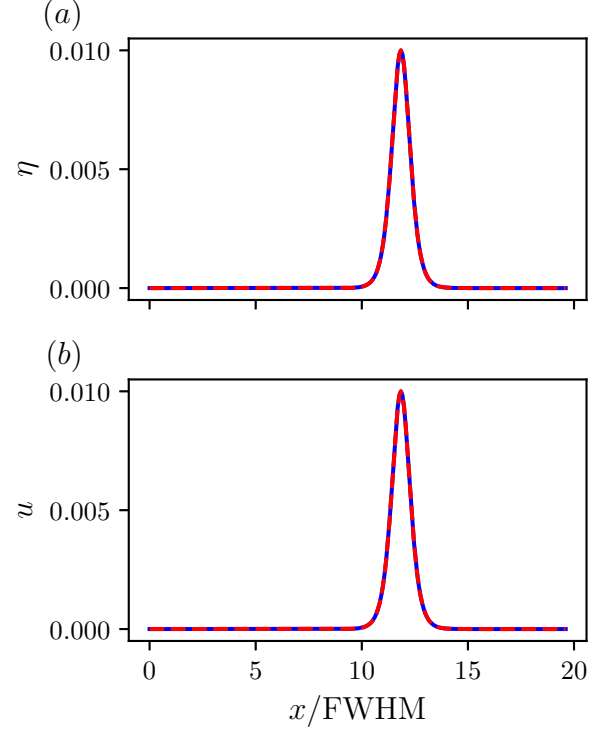


Figure 11. Comparison of the numerical (solid blue) and analytical (dashed red) solutions for (a) velocity and (b) surface elevation for the full KB system at $t = 2\tau_s$.

with $c = 1.005$. We characterize the time scale of the system by the pulse duration $\tau_s = \text{FWHM}/c$ where FWHM is the full width at half-maximum for the soliton profile and c is the soliton velocity. We allow the soliton to propagate for $2\tau_s$. Figure 11 shows a comparison between the numerical and analytical solutions at $2\tau_s$, demonstrating the high accuracy of the numerical results. We test the conservation of two quantities, the total energy H and the total momentum P , defined by the integrals

$$H(t) = \int E(x, t) dx, \quad P(t) = \int I(x, t) dx. \quad (\text{F12})$$

For the KB system, the energy density E is expressed as

$$E = \frac{\alpha^2}{2}\eta^2 + \frac{\alpha^2}{2}(1+\alpha\eta)w^2 + \frac{\alpha^2\beta}{3}ww_{xx} + \frac{\alpha^2\beta}{6}w_x^2, \quad (\text{F13})$$

and the momentum density I takes the form

$$I = \alpha w + \alpha^2 w\eta + \frac{1}{3}\alpha\beta w_{xx}, \quad (\text{F14})$$

as presented in [46]. Figure 12 demonstrates that the energy H and the momentum P remain constant for the duration of the simulation.

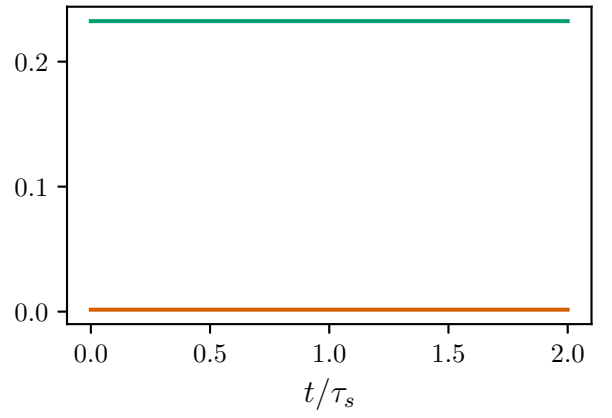


Figure 12. Total momentum P (green line) and energy H (orange line) plotted at each time step over the duration of $2\tau_s$ for the full KB system.

3. Validation of KdV Equation

We begin by considering the linear part of the KdV equation. Setting $\alpha = 0$ in (E1) leaves

$$\eta_t + \eta_x + \frac{1}{6}\beta\eta_{xxx} = 0, \quad (\text{F15})$$

which has an analytical solution of the form $\eta(x, t) = \sin(kx - wt)$ with $\omega = k - \frac{\beta}{6}k^3$. For this test case, we set $\beta = 1$ and use (F15) with $t = 0$ as our initial condition. Figure 13 compares the numerical and analytical solutions after $10T_p$. As expected from the integrating factor scheme used, the surface elevation agrees with the analytical result up to machine precision. Proceeding with

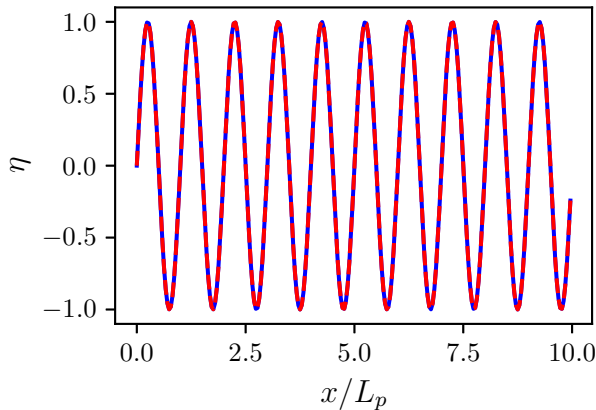


Figure 13. Comparison of the numerical (solid blue) and analytical (red dashed line) solutions for velocity (top panel) and surface elevation (bottom panel) for the linear portion of the KdV equation at $t = 10T_p$.

the full KdV equation, we set $\alpha = \beta = 1$ and take a known soliton solution

$$\eta(x, t) = 2(c-1) \operatorname{sech}^2 \left[\sqrt{\frac{3}{2}(c-1)} (x - ct) \right] \quad (\text{F16})$$

with $c = 1.005$ and $t = 0$ for our initial condition. We follow the same procedure as in F 2 by defining the time scale in terms of τ_s . Figure 14 illustrates the high degree of precision between the numerical and analytical solutions. Conservation of total energy H and total momentum E for KdV is also validated using the integrals defined in (F12); however, in this case the energy density is defined as

$$E = \alpha^2 \eta^2 + \frac{\alpha^3}{4} \eta^3 + \frac{\alpha^2 \beta}{6} \eta \eta_{xx} + \frac{\alpha^2 \beta}{6} \eta_x^2, \quad (\text{F17})$$

while the momentum density is

$$I = \alpha \eta + \frac{3}{4} \alpha^2 \eta^2 + \frac{1}{6} \alpha \beta \eta_{xx}, \quad (\text{F18})$$

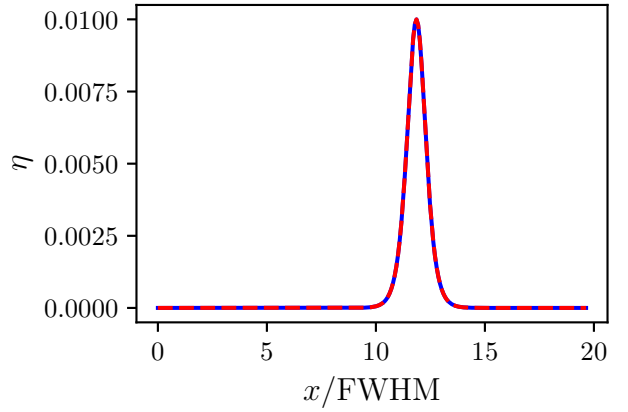


Figure 14. Comparison of the numerical (solid blue) and analytical (dashed red) solutions for velocity (top panel) and surface elevation (bottom panel) for the full KdV equation at $t = 2\tau_s$.

as derived in [47]. Figure 15 confirms the conservation of both energy H and momentum P for the duration of the simulation.

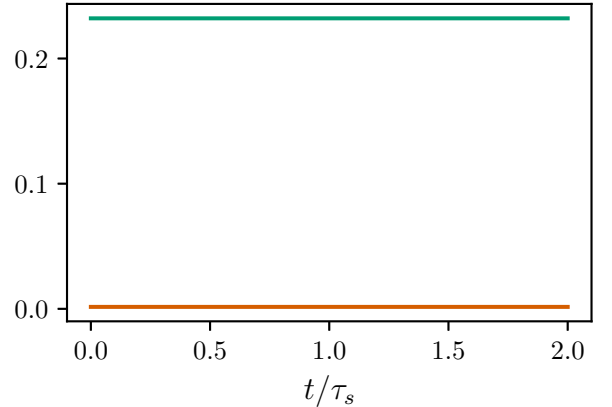


Figure 15. Total momentum P (green line) and energy H (orange line) plotted at each time step over the duration of $2\tau_s$ for the full KdV equation.

Appendix G: Numerical scheme for DST

We solve (52) using a finite-difference method on a uniform grid $x_j = -L/2 + j\Delta x$, $j = 0, \dots, N-1$ and $\Delta x = L/(N-1)$. Defining the grid values by $\Psi_j = \Psi(x_j)$, we approximate $\Psi_{xx}(x_j)$ at the interior points $j = 1, \dots, N-2$ using a second-order central difference stencil

$$\frac{\Psi_{j-1} - 2\Psi_j + \Psi_{j+1}}{\Delta x^2} + V_j \Psi_j = 0 \quad (\text{G1})$$

where $V_j := E(\zeta)^2 + ik(\zeta)q(x_j) + r(x_j)$. To capture bound states (elements of the discrete spectrum), we impose asymptotically decaying boundary conditions. That is, for sufficiently large $|x|$

$$\Psi(x) \sim e^{(-iE|x|)}, \quad \text{Im}[E] > 0,$$

so that

$$\Psi_x(x) \sim -iE \operatorname{sgn}(x) \Psi(x).$$

The requirement of $\text{Im}[E] > 0$ places us in the upper half E -plane, which ensures decay. These asymptotics lead to Robin boundary conditions

$$\Psi_x(-L/2) - iE\Psi(-L/2) = 0, \quad \Psi_x(L/2) + iE\Psi(L/2) = 0.$$

These boundary conditions are applied with second-order one-sided finite differences at the end points. At the left boundary, we use the forward stencil

$$\frac{-3\Psi_0 + 4\Psi_1 - \Psi_2}{2\Delta x} - iE\Psi_0 = 0, \quad (\text{G2})$$

and at the right boundary we use the backward stencil

$$\frac{3\Psi_{N-1} - 4\Psi_{N-2} + \Psi_{N-3}}{2\Delta x} + iE\Psi_{N-1} = 0. \quad (\text{G3})$$

By assembling (G1), (G2), (G3) we obtain a $N \times N$ linear system $A(\zeta)\Psi = 0$. The majority of the matrix $A(\zeta)$ consists of tridiagonal entries corresponding to the interior discretization, while the boundary conditions are incorporated by modifying the matrix's first and last rows. Bound states correspond to values of ζ for which $A(\zeta)$ is singular, i.e.,

$$\det A(\zeta) = 0,$$

defining a nonlinear eigenvalue problem. Instead of evaluating $\det A(\zeta)$ directly, we locate roots via a Newton iteration of the smallest singular value of $A(\zeta)$ (as zeros of the determinant correspond to points where the smallest singular value is zero). At each iterate ζ , the singular value decomposition $A(\zeta) = U\Sigma V^*$ is computed. From this, we extract the minimal singular value

$\sigma := \sigma_{\min}(A(\zeta))$ and its corresponding left and right singular vectors u and v , respectively. We can then define the derivative as $d\sigma/d\zeta = u^* A'(\zeta) v$ where $A'(\zeta)$ is simply the derivative of the matrix $A(\zeta)$ with respect to ζ [48]. The update formula is given by

$$d\zeta = -\frac{\sigma}{u^* A'(\zeta) v}$$

so that $\zeta \leftarrow \zeta + d\zeta$ at each iteration. We iterate until σ falls below some prescribed tolerance, indicating that a root has been located. To ensure robust identification of all roots, we implement a multi-start Newton's method by selecting the initial value of ζ from a sufficiently fine mesh spanning the complex ζ -plane. We remark that for $\beta > 0$, bound states correspond either to purely imaginary eigenvalues ($\zeta = i\eta$, $\eta \in \mathbb{R}$), or to complex-conjugate pairs ($\zeta_2 = -\zeta_1^*$), as in the case of breathers in the Sine-Gordon equation [3].

The criterion for the robustness of bound states corresponding to solitons can be stated in terms of the soliton velocity. The velocity profile for a KB soliton is given by

$$u(x, t) = \frac{2(c_s^2 - 1)}{\alpha \cosh(\sqrt{\frac{3}{\beta}(c_s^2 - 1)}(x - c_s t)) + c_s}, \quad (\text{G4})$$

where c_s is the soliton velocity, which can be computed via the discrete eigenvalues ζ [3]. To ensure physical realizability, the soliton velocity must satisfy $|c_s| > 1$. This condition ensures that the quantity K corresponding to

$\sqrt{\frac{3}{\beta}(c_s^2 - 1)}$ appearing in the hyperbolic cosine argument of (G4) remains real and positive. The parameter K controls the inverse width of the soliton profile, i.e., width $\propto 1/K$; therefore, solitons with velocities closer to 1 (corresponding to eigenvalues closer to the continuous spectrum) exhibit broad profiles with slow decay in the physical domain. These solitons are not expected to be realized in our finite domain due to their excessive width. Solitons with larger velocities correspond to narrower, more strongly localized solitons. This is consistent with the definition of “true” bound states where the tails decay to zero as $|x| \rightarrow \infty$. The condition of $|c_s| > 1$ is satisfied for $-3i < \zeta < 0$ and $5i < \zeta < i\infty$. Any discrete eigenvalue that does not satisfy this condition is deemed spurious and is not included in the computation of the soliton energy presented in §III B 1.

-
- [1] V. E. Zakharov, V. S. L'vov, and G. Falkovich, *Kolmogorov spectra of turbulence I: Wave turbulence* (Springer Science & Business Media, 2012).
- [2] S. Nazarenko, *Wave Turbulence* (Springer Berlin Heidelberg, 2011).
- [3] D. J. Kaup, A Higher-Order Water-Wave Equation and the Method for Solving It, *Progress of Theoretical Physics* **54**, 396 (1975).
- [4] B. A. Kupershmidt, Mathematics of dispersive water waves, *Communications in Mathematical Physics* **99**, 51–73 (1985).
- [5] G. A. El, R. H. J. Grimshaw, and M. V. Pavlov, In-

- tegrable Shallow-Water Equations and Undular Bores, *Studies in Applied Mathematics* **106**, 157–186 (2001).
- [6] R. Ivanov, Two-component integrable systems modelling shallow water waves: The constant vorticity case, *Wave Motion* **46**, 389–396 (2009).
- [7] A. H. Bhrawy, M. M. Tharwat, and M. A. Abdelkawy, Integrable system modelling shallow water waves: Kaup–boussinesq shallow water system, *Indian Journal of Physics* **87**, 665–671 (2013).
- [8] R. Gong and D.-S. Wang, Formation of the undular bores in shallow water generalized Kaup–Boussinesq model, *Physica D: Nonlinear Phenomena* **439**, 133398 (2022).
- [9] V. E. Zakharov, Turbulence in Integrable Systems, *Studies in Applied Mathematics* **122**, 219–234 (2009).
- [10] K. Hasselmann, On the non-linear energy transfer in a gravity-wave spectrum Part 1. General theory, *Journal of Fluid Mechanics* **12**, 481–500 (1962).
- [11] A. Dyachenko, Y. Lvov, and V. Zakharov, Five-wave interaction on the surface of deep fluid, *Physica D: Nonlinear Phenomena* **87**, 233–261 (1995).
- [12] Y. Lvov, Effective five-wave Hamiltonian for surface water waves, *Physics Letters A* **230**, 38 (1997).
- [13] D. Lucas, M. Perlin, D.-Y. Liu, S. Walsh, R. Ivanov, and M. D. Bustamante, Five-Wave Resonances in Deep Water Gravity Waves: Integrability, Numerical Simulations and Experiments, *Fluids* **6**, 205 (2021).
- [14] O. M. Phillips, On the dynamics of unsteady gravity waves of finite amplitude Part 1. The elementary interactions, *Journal of Fluid Mechanics* **9**, 193–217 (1960).
- [15] M. S. Longuet-Higgins, Resonant interactions between two trains of gravity waves, *Journal of Fluid Mechanics* **12**, 321–332 (1962).
- [16] V. E. Zakharov, Stability of periodic waves of finite amplitude on the surface of a deep fluid, *Journal of Applied Mechanics and Technical Physics* **9**, 190–194 (1968).
- [17] V. Zakharov, Statistical theory of gravity and capillary waves on the surface of a finite-depth fluid, *European Journal of Mechanics - B/Fluids* **18**, 327 (1999), three-Dimensional Aspects of Air-Sea Interaction.
- [18] M. Onorato, A. R. Osborne, P. Janssen, and D. Resio, Four-wave resonant interactions in the classical quadratic Boussinesq equations, *Journal of Fluid Mechanics* **618**, 263 (2009).
- [19] J. M. Kaihatu, J. Veeramony, K. L. Edwards, and J. T. Kirby, Asymptotic behavior of frequency and wave number spectra of nearshore shoaling and breaking waves, *Journal of Geophysical Research: Oceans* **112** (2007).
- [20] I. Redor, E. Barthélémy, H. Michallet, M. Onorato, and N. Mordant, Experimental Evidence of a Hydrodynamic Soliton Gas, *Phys. Rev. Lett.* **122**, 214502 (2019).
- [21] I. Redor, H. Michallet, N. Mordant, and E. Barthélémy, Experimental study of integrable turbulence in shallow water, *Physical Review Fluids* **6**, 124801 (2021).
- [22] T. Leducque, M. Kaczmarek, H. Michallet, E. Barthélémy, and N. Mordant, From deep to shallow water two-dimensional wave turbulence: Emergence of soliton gas, *Phys. Rev. Fluids* **10**, 114801 (2025).
- [23] E. Pelinovsky and A. Sergeeva (Kokorina), Numerical modeling of the KdV random wave field, *European Journal of Mechanics - B/Fluids* **25**, 425 (2006).
- [24] D. S. Agafontsev and V. E. Zakharov, Integrable turbulence and formation of rogue waves, *Nonlinearity* **28**, 2791 (2015).
- [25] D. S. Agafontsev and V. E. Zakharov, Integrable turbulence generated from modulational instability of cnoidal waves, *Nonlinearity* **29**, 3551 (2016).
- [26] S. Randoux, P. Walczak, M. Onorato, and P. Suret, Nonlinear random optical waves: Integrable turbulence, rogue waves and intermittency, *Physica D: Nonlinear Phenomena* **333**, 323 (2016), dispersive Hydrodynamics.
- [27] G. Roberti, G. El, S. Randoux, and P. Suret, Early stage of integrable turbulence in the one-dimensional nonlinear Schrödinger equation: A semiclassical approach to statistics, *Phys. Rev. E* **100**, 032212 (2019).
- [28] G. A. El, Soliton gas in integrable dispersive hydrodynamics, *Journal of Statistical Mechanics: Theory and Experiment* **2021**, 114001 (2021).
- [29] T. Bonnemain, B. Doyon, and G. El, Generalized hydrodynamics of the KdV soliton gas, *Journal of Physics A: Mathematical and Theoretical* **55**, 374004 (2022).
- [30] P. Suret, S. Randoux, A. Gelash, D. Agafontsev, B. Doyon, and G. El, Soliton gas: Theory, numerics, and experiments, *Phys. Rev. E* **109**, 061001 (2024).
- [31] M. Onorato, L. Vozella, D. Proment, and Y. V. Lvov, Route to thermalization in the α -Fermi–Pasta–Ulam system, *Proceedings of the National Academy of Sciences* **112**, 4208–4213 (2015).
- [32] V. P. Krasitskii, On reduced equations in the Hamiltonian theory of weakly nonlinear surface waves, *Journal of Fluid Mechanics* **272**, 1–20 (1994).
- [33] B. Wu, M. Onorato, Z. Hani, and Y. Pan, Validity condition of normal form transformation for the β -FPUT system (2025), arXiv:2510.04831 [math-ph].
- [34] Y. Pan, High-order spectral method for the simulation of capillary waves with complete order consistency, *Journal of Computational Physics* **408**, 109299 (2020).
- [35] M. V. Flamanion and E. Pelinovsky, Nonlinear random wave fields within a Boussinesq system, *Physics Letters A* **520**, 129677 (2024).
- [36] A. I. Dyachenko, A. O. Korotkevich, and V. E. Zakharov, Weak Turbulent Kolmogorov Spectrum for Surface Gravity Waves, *Phys. Rev. Lett.* **92**, 134501 (2004).
- [37] Z. Zhang and Y. Pan, Numerical investigation of turbulence of surface gravity waves, *Journal of Fluid Mechanics* **933**, A58 (2022).
- [38] A. O. Korotkevich, Inverse Cascade Spectrum of Gravity Waves in the Presence of a Condensate: A Direct Numerical Simulation, *Phys. Rev. Lett.* **130**, 264002 (2023).
- [39] V. S. L'vov and S. Nazarenko, Discrete and mesoscopic regimes of finite-size wave turbulence, *Physical Review E* **82**, 056322 (2010).
- [40] A. Hrabski and Y. Pan, Effect of discrete resonant manifold structure on discrete wave turbulence, *Physical Review E* **102**, 041101 (2020).
- [41] Z. Zhang and Y. Pan, Forward and inverse cascades by exact resonances in surface gravity waves, *Physical Review E* **106**, 044213 (2022).
- [42] C. Colléaux, J. Skipp, S. Nazarenko, and J. Laurie, A bound state attractor in optical turbulence, *Physica D: Nonlinear Phenomena* **477**, 134687 (2025).
- [43] A. Karczewska and P. Rozmej, *Shallow water waves: Extended Kortweg-de Vries equations: Second order perturbation approach* (Oficyna Wydawnicza Uniwersytetu Zielonogórskiego, 2018).
- [44] L. N. Trefethen, *Spectral Methods in MATLAB* (Society for Industrial and Applied Mathematics, 2000).
- [45] B.-S. H. Juliussen, *Investigations of the Kaup-Boussinesq model equations for water waves*, Master thesis, The Uni-

- versity of Bergen (2014).
- [46] Ali, A., Juliussen, B.-S., and Kalisch, H., Approximate Conservation Laws for an Integrable Boussinesq System, *Math. Model. Nat. Phenom.* **12**, 1 (2017).
- [47] A. Ali and H. Kalisch, On the Formulation of Mass, Momentum and Energy Conservation in the KdV Equation, *Acta Applicandae Mathematicae* **133**, 113–131 (2013).
- [48] X.-P. Chen and H. Dai, A modified newton method for nonlinear eigenvalue problems, *East Asian Journal on Applied Mathematics* **8**, 139–150 (2018).